



Different contact angle distributions for heterogeneous ice nucleation in the Community Atmospheric Model version 5

Y. Wang^{1,2,3}, X. Liu², C. Hoose⁴, and B. Wang^{1,5}

¹State Key Laboratory of Numerical Modeling for Atmospheric Sciences and Geophysical Fluid Dynamics (LASG), Institute of Atmospheric Physics, Chinese Academy of Sciences, Beijing 100029, China

²Department of Atmospheric Science, University of Wyoming, Laramie, WY 82071, USA

³College of Earth Science, University of Chinese Academy of Sciences, Beijing 100049, China

⁴Karlsruhe Institute of Technology, Institute for Meteorology and Climate Research, 76131 Karlsruhe, Germany

⁵Ministry of Education Key Laboratory for Earth System Modeling, Center of Earth System Science (CESS), Tsinghua University, Beijing 100084, China

Correspondence to: X. Liu (xliu6@uwoyo.edu)

Received: 4 March 2014 – Published in Atmos. Chem. Phys. Discuss.: 18 March 2014

Revised: 7 July 2014 – Accepted: 15 August 2014 – Published: 1 October 2014

Abstract. In order to investigate the impact of different treatments for the contact angle (α) in heterogeneous ice nucleating properties of natural dust and black carbon (BC) particles, we implement the classical-nucleation-theory-based parameterization of heterogeneous ice nucleation (Hoose et al., 2010) in the Community Atmospheric Model version 5 (CAM5) and then improve it by replacing the original single-contact-angle model with the probability-density-function-of- α (α -PDF) model to better represent the ice nucleation behavior of natural dust found in observations. We refit the classical nucleation theory (CNT) to constrain the uncertain parameters (i.e., onset α and activation energy in the single- α model; mean contact angle and standard deviation in the α -PDF model) using recent observation data sets for Saharan natural dust and BC (soot). We investigate the impact of the time dependence of droplet freezing on mixed-phase clouds and climate in CAM5 as well as the roles of natural dust and soot in different nucleation mechanisms. Our results show that, when compared with observations, the potential ice nuclei (IN) calculated by the α -PDF model show better agreement than those calculated by the single- α model at warm temperatures (T ; $T > -20^\circ\text{C}$). More ice crystals can form at low altitudes (with warm temperatures) simulated by the α -PDF model than compared to the single- α model in CAM5. All of these can be attributed to different ice nucleation efficiencies among aerosol particles, with some particles having smaller contact angles (higher efficiencies) in the α -PDF

model. In the sensitivity tests with the α -PDF model, we find that the change in mean contact angle has a larger impact on the active fraction at a given temperature than a change in standard deviation, even though the change in standard deviation can lead to a change in freezing behavior. Both the single- α and the α -PDF model indicate that the immersion freezing of natural dust plays a more important role in the heterogeneous nucleation than that of soot in mixed-phase clouds. The new parameterizations implemented in CAM5 induce more significant aerosol indirect effects than the default parameterization.

1 Introduction

Ice microphysical processes in clouds are vital to cloud radiative properties and precipitation formation. They include primary ice formation, vapor deposition on ice crystals, accretion of cloud droplets by ice crystals, ice aggregation and sedimentation, ice multiplication, sublimation, melting, and convective detrainment of cloud ice (Pruppacher and Klett, 1997; Morrison and Gettelman, 2008). Until now, ice formation mechanisms, especially heterogeneous ice nucleation, have not been well understood. In mixed-phase clouds with temperatures between 0 and -38°C , primary ice formation can be via heterogeneous ice nucleation with the aid of a fraction of aerosol particles called ice nuclei (IN) (DeMott et al.,

2010). Various particles can act as IN, which include mineral dust, soot, volcanic ash and primary biological particles (Hoose and Möhler, 2012; Murray et al., 2012).

Mineral dust has been recognized as the most important, atmospherically relevant IN in laboratory measurements and field sample studies (Hoose and Möhler, 2012; Murray et al., 2012). Natural mineral dust particles are often internally mixed, consisting of different minerals, quartz and other components (Murray et al., 2012). In order to reduce the complexity encountered in natural mineral dusts, many laboratory studies have, on the one hand, often used commercially available minerals, in particular kaolinite, illite and montmorillonite (Hoose et al., 2008; Hoose and Möhler, 2012). On the other hand, other laboratory experiments used commercially available Arizona test dust (ATD) as a surrogate for natural mineral dusts (e.g., Knopf and Koop, 2006; Marcolli et al., 2007; Kulkarni et al., 2012). ATD can possibly be more ice nucleation active than natural desert dust, either due to its enhanced roughness resulting from milling or due to its different mineralogical composition (Möhler et al., 2006). Another reason for lower activity of natural dust particles is related to their aging processes in the atmosphere, which may reduce their ice nucleation ability (Sullivan et al., 2010).

Heterogeneous ice nucleation occurs via several different mechanisms (Vali, 1985), called nucleation modes (immersion, deposition, condensation and contact freezing). For immersion freezing, a supercooled cloud droplet containing an ice nucleus nucleates by further cooling to a certain temperature. Using airborne measurements of IN number concentration and elemental composition from the US Department of Energy (DOE) Atmospheric Radiation Measurement (ARM) Mixed-Phase Arctic Clouds Experiment (M-PACE) in northern Alaska, Prenni et al. (2007) found that immersion and/or condensation freezing (instruments can not distinguish between them) may be the dominant freezing mechanism within these clouds. The term “deposition nucleation” describes the vapor phase being deposited directly onto a dry ice nucleus, which leads to the growth of ice. “Contact freezing” refers to the freezing of a supercooled droplet which collides with a dry ice nucleus.

To represent the heterogeneous IN number and ice nucleation process, several heterogeneous freezing parameterizations have been developed, which can be divided into two types: the singular (or deterministic) hypothesis and the stochastic hypothesis. The first, “singular (or deterministic) hypothesis”, proposed by Langham and Mason (1958), assumes that the radius of the ice germ forming on the aerosol surface at a given supercooling is controlled by surface features and that thermal fluctuations have a negligible influence on the ice germ radius. Thus, the freezing of a droplet is only determined by whether the temperature is below the characteristic temperature of the immersed IN in the droplet (Phillips et al., 2008, 2012; DeMott et al., 2010; Niedermeier et al., 2010; Niemand et al., 2012). The second hypothesis,

the “stochastic hypothesis” proposed by Bigg (1953), holds that heterogeneous ice nucleation is a function of time. During the time an immersed aerosol particle spends at a constant environmental temperature, water molecules within supercooled water stay in the thermal fluctuation state of capturing and losing molecules to produce a cluster. This cluster resembles the structure of ice. When some of these ice germs reach a certain size (the critical radius), they become stable and initiate freezing. The presence of a particle surface immersed in a supercooled droplet is helpful for ice formation by reducing the number of water molecules that are required to reach the stable cluster radius by letting the germ form on the particle surface as a spherical cap. The rate of heterogeneous nucleation per aerosol particle and per time is referred to as the nucleation rate (J_{het}). This stochastic approach can be described by classical nucleation theory (CNT) (Chen et al., 2008; Hoose et al., 2010; Niedermeier et al., 2011; Welti et al., 2012).

In CNT, J_{het} is proportional to the aerosol surface area and is a function of the contact angle (α), which is the angle where the ice-germ–liquid or ice-germ–vapor interface meets the aerosol surface; J_{het} can be understood as the surrogate of the nucleation ability of aerosol particles. The particle with the smaller contact angle (α) has a higher ice nucleating efficiency. The contact angle is often derived from the fitting to the laboratory data, as done in Marcolli et al. (2007) for ATD, in Lüönd et al. (2010) for kaolinite and in Wheeler and Bertram (2012) for kaolinite and illite. As noted in these studies, assuming that each particle has the same fixed contact angle often does not fit the observation data well, especially when the observed ice nucleating fraction increases slowly with the increase in time (Welti et al., 2012). These authors (Marcolli et al., 2007; Lüönd et al., 2010; Wheeler and Bertram, 2012; Welti et al., 2012) suggested using a probability density function of contact angles (α -PDF) instead of single values to better fit the observed frozen fraction as a function of temperature (for immersion/condensation nucleation) or supersaturation (for deposition nucleation). In this α -PDF model, contact angles are distributed to every particle, which means that each particle has one value for the contact angle and that the particles with low contact angles are rapidly depleted when the temperature is held constant, thus leading to a slowdown of the freezing of the sample. The α -PDF model can be interpreted as an “intermediate” approach based on CNT between the two extremes of stochastic and singular hypotheses (Niedermeier et al., 2010).

Several heterogeneous ice nucleation parameterizations which are based on laboratory studies or in situ measurements have been implemented in global climate models (GCMs). Liu et al. (2007) implemented Meyers et al. (1992) in Community Atmospheric Model version 3 (CAM3) and in Community Atmospheric Model version 5 (CAM5; Gettelman et al., 2010) for the immersion, condensation and deposition mechanisms. Xie et al. (2013) evaluated the DeMott et al. (2010) parameterization in CAM5, comparing it

to Meyers et al. (1992). Lohmann and Diehl (2006) implemented the Diehl and Wurzler (2004) parameterization in the global climate model of the Max Planck Institute for Meteorology (European Center/Hamburg Model version 5; ECHAM5) for the immersion freezing of cloud droplets. Hoose et al. (2010) implemented the CNT in Community Atmosphere Model version 3 (CAM3)-Oslo for the immersion, deposition and contact freezing of dust, soot and biological aerosols. In their paper, they suggest that assuming stochastic ice nucleation with all particles having the same fixed single contact angle does not fit some observations very well. Immersion freezing and deposition nucleation by dust in Hoose et al. (2010) are fitted to the observation data obtained specifically for montmorillonite (Pitter and Pruppacher, 1973) and illite (Zimmermann et al., 2008), respectively. Thus their results may not reflect ice nucleation behavior by natural dust particles, which are mixtures of complex mineral components.

In this study, we implement the single- α model (Hoose et al. 2010) in CAM5 to represent the heterogeneous ice nucleation of natural dust and BC in mixed-phase clouds. The single- α model is further improved by the α -PDF model to correct the time-dependent behavior of droplet freezing. To better represent the ice nucleation of natural dust found in ambient observations, we use recent observation data on Saharan dust to constrain the parameters used in the CNT parameterization. The model description is presented in Sect. 2. Section 3 describes the CNT parameterizations, with the resulting fitting parameters. In Sect. 4, the model experiments and results are presented. Uncertainties and implications are discussed in Sect. 5.

2 CAM5

CAM5 includes a two-moment stratiform cloud microphysics scheme (Morrison and Gettelman 2008 (MG08); Gettelman et al., 2008, 2010). This scheme predicts number concentrations and mass mixing ratios of cloud droplets and ice crystals; the number concentrations and mass mixing ratios of snow and rain are also determined. MG08 treats the microphysical conversions among cloud liquid droplets, ice crystals, rain and snow. As for cloud droplet activation, it follows the Abdul-Razzak and Ghan (2000) parameterization. MG08 was further updated in CAM5 (Gettelman et al., 2010) to implement the Liu et al. (2007) scheme for ice crystal nucleation in mixed-phase and cirrus clouds. In mixed-phase clouds, Meyers et al. (1992) is used for deposition, immersion and condensation freezing of cloud droplets; it does not, however, provide a link between IN number concentration and aerosol properties. In addition, the Young (1974) scheme is used for contact freezing of cloud droplets due to coarse-mode dust.

CAM5 includes a modal aerosol module (MAM) to represent aerosol processes and properties in the atmosphere

(Liu et al., 2012a). It predicts aerosol number concentrations and mass mixing ratios of multiple aerosol species in three aerosol modes: Aitken, accumulation and coarse mode. MAM treats major aerosol species including mineral dust, BC, sea salt, sulfate, and primary and secondary organic aerosols. These aerosol species are internally mixed within a single mode but externally mixed between different modes. Aerosol species in cloud-borne states are also explicitly treated but not predicted in the model.

The deep-convection scheme in CAM5 follows Zhang and McFarlane (1995) but with the diluted convective available potential energy (CAPE) modification described in Neale et al. (2008). The shallow-convection scheme is from Park and Bretherton (2009). The stratus–radiation–turbulence interactions in CAM5 are explicitly simulated by the moist turbulence scheme (Bretherton and Park, 2009). The radiative transfer calculations for aerosol and cloud radiative effects are based on the Rapid Radiative Transfer Model for GCMs (RRTMG) (Iacono et al., 2008).

3 New heterogeneous ice nucleation parameterization in CAM5

3.1 Single-contact-angle (α) model

In the CNT, ice nucleation is treated as a stochastic process (Pruppacher and Klett, 1997). An energy barrier has to be passed to capture more molecules to form small agglomerates of ice (subcritical germs) on the surface of an ice nucleus until a critical germ size is reached. Following the remarks in Hoose et al. (2010), both deposition and immersion freezing can be treated in the same general form based on the CNT. Following the suggestion of Chen et al. (2008), we calculate contact freezing with the critical germ radius of immersion freezing and the homogeneous energy of germ formation in deposition freezing according to “Cooper’s hypothesis” (Cooper, 1974).

We modify the original expression used in Hoose et al. (2010) concerning J_{het} (the rate of heterogeneous nucleation per aerosol particle and per second) with the form factor (f) raised to the $-1/2$ power instead of $1/2$ (see Eq. 1); this is done due to the unphysical behavior of the original expression which implies that $J_{\text{het}} \rightarrow 0$ when $f \rightarrow 0$ (i.e., the ice nucleation rate will become smaller on more easily wettable materials) (Määttä et al., 2005; Barahona, 2012).

$$J_{\text{het}} = \frac{A' r_N^2}{\sqrt{f}} \exp\left(\frac{-\Delta g^\# - f \Delta g_g^o}{kT}\right), \quad (1)$$

where A' is a prefactor, r_N is the aerosol particle radius, f is a form factor containing information about the aerosol’s ice nucleation ability, $\Delta g^\#$ is the activation energy, Δg_g^o is the homogeneous energy of germ formation, k is the Boltzmann constant and T is the temperature in K.

The second modification concerns f itself. Due to the uncertainty of assuming a spherical substrate (or any other simple geometry) (Barahona, 2012) and due to the fact that the difference between a flat surface and a spherical surface can be ignored when the diameter of a particle is larger than 100 nm, we calculate the compatibility parameter f with a flat surface instead of the convex surface. Thus, f has the form (Pruppacher and Klett, 1997)

$$f = \frac{1}{4}(2+m)(1-m)^2, \quad (2)$$

where $m \equiv \cos \alpha$ and α is the contact angle.

Except for the above changes, detailed descriptions of the formulation of CNT for immersion, deposition and contact freezing can be found in Hoose et al. (2010). We note that Hoose et al. (2010) used the activation fraction of aerosols, which is diagnosed from the droplet activation parameterization, to divide dust and soot number concentrations in each grid into the interstitial portion for deposition and contact freezing and into the cloud-borne portion for immersion freezing. However, in CAM5 we use the interstitial and cloud-borne dust and soot number concentrations directly in the ice nucleation calculation, since CAM5 explicitly treats these two states of aerosols.

3.2 α -PDF model

We consider the α -PDF model for immersion freezing by natural dust in order to replace the single- α model in Hoose et al. (2010). In the α -PDF model, we can take the heterogeneity of individual particles in the aerosol population into account. The particle surface is still uniform in the ice nucleation property for each particle but differs within an ensemble of particle population by a distribution of different contact angles. The distribution of contact angles is assumed to follow a log-normal probability density function (Marcolli et al., 2007; Lüönd et al., 2010).

The log-normal probability density function which represents the occurrence probability of one contact angle for one particle is given by

$$p(\alpha) = \frac{1}{\alpha\sigma\sqrt{2\pi}} \exp\left(-\frac{(\ln(\alpha) - \ln(\mu))^2}{2\sigma^2}\right), \quad (3)$$

where μ is the mean contact angle and σ is the standard deviation.

The frozen fraction for a given temperature can then be calculated as

$$f_{\text{act},\alpha\text{-pdf}} = 1 - \int_0^\pi p(\alpha) \cdot \exp(-J_{\text{imm}}(T, \alpha)\Delta t) d\alpha. \quad (4)$$

Here J_{imm} is the immersion nucleation rate for one particle with one certain contact angle, and Δt is the model time step.

It should be mentioned that, in the global climate model, different time dependencies of the frozen fraction in the single- α model and the α -PDF model are only treated within one time step. In the current CAM5 model, because of the added complexity and the computational demands, aerosol scavenging due to droplet freezing is not taken into account. This means that only if the active fractions are large enough in the last time step would additional (and unphysical) ice nucleation occur in the following time step with both contact angle distributions if temperature is constant. Especially for the α -PDF model, as particles with small contact angles are not scavenged in each time step, these small contact angles can not be tracked with time in the model to adjust the distribution of the contact angle (adding even more complexity). However, since we use predicted cloud-borne dust and BC directly, cloud-borne aerosols will be updated during each model time step (30 min), which means that fresh particles, such as cloud condensation nuclei (CCN), will be nucleated into cloud droplets. As the new parameterizations implemented in this study predict that the active fractions due to droplet freezing in one model time step of 30 min are much smaller than 100 % (see, e.g., Fig. 2), these newly formed cloud droplets are sufficient to make up the depleted amounts of cloud droplets (i.e., Δt in Eq. (4) may be also thought of as a timescale to replenish IN population in a grid point). Moreover, after the Wegener–Bergeron–Findeisen process sets in, further ice nucleation will be suppressed. Overall, in this case we actually benefit from the long time step because the clouds and the environmental conditions change significantly from time step to time step, such that starting afresh is not a bad assumption. In particular, entrainment of new IN, temperature changes and the shutdown of ice nucleation through the Bergeron process are thought to be important. Therefore, the new parameterizations only have a small artifact due to the absence of aerosol scavenging because of droplet freezing and the assumption that there is a constant distribution of contact angles in the α -PDF model among time steps. Another point is that new parameterizations in the CAM5 model reduce nucleated ice crystals when compared to the default Meyers et al. scheme (see Table 4), which means that the depletion of cloud-borne aerosols has a smaller effect on model results than the default scheme.

3.3 Fitting parameters for natural dust and soot

Fitting parameters in the CNT, such as the single contact angle (α) and activation energy ($\Delta g^\#$) in the single- α model, can be derived by minimizing the root mean square error (RMSE) of frozen fractions between observation data and model results. Thus the RMSE is calculated as

$$\text{RMSE} = \sqrt{\frac{1}{N} \sum_1^N [F_{\text{ice}} - F_{\text{ice}}^{\text{mod}}]^2}, \quad (5)$$

where F_{ice} is the observed frozen fraction, $F_{\text{ice}}^{\text{mod}}$ is the frozen fraction calculated from the single- α model and N is the total number of observation data points.

The formula to derive uncertain parameters in the α -PDF approach is the same as Eq. (5) except that we calculate $F_{\text{ice}}^{\text{mod}}$ from the α -PDF model. In order to calculate $F_{\text{ice}}^{\text{mod}}$, its integral form of Eq. (4) was discretized into 2000 bins, and then the PDF distribution parameters, standard deviation (σ) and mean contact angle (μ) were iterated to find the best fit following Eq. (5).

The resulting fitting parameters for the immersion and deposition freezing based on the single- α model are listed in Table 1. Observation data for the immersion freezing of dust are obtained from the Colorado State University CFDC (continuous-flow diffusion chamber)-HIAPER version 1 (CSU CFDC-1H) experiment, which is selected for the 106 % (CSU106) relative humidity with respect to water (RH_w) (DeMott et al., 2011); data for the deposition freezing on dust are from the laboratory study in Koehler et al. (2010). Both of the two studies used samples for Saharan dust, which generally contains quartz, feldspars and clay minerals in different compositions (Linke et al., 2006). The immersion and deposition by soot are still based on the measurements (DeMott, 1990; Möhler et al., 2005) used in Hoose et al. (2010). However, due to the modification of the expressions J_{het} and f in Sect. 3.1, we refit uncertain parameters in the single- α model to these data again. In the case of deposition freezing in Table 1, Δg^\ddagger is negative and the reason is as follows. Δg^\ddagger (activation energy) is the energy of desorption per molecule, which stands for the surface with an outward flux of desorbed molecules. However, J_{het} specifies the flux of water molecules to the germs. There should not actually be a negative sign before Δg^\ddagger in J_{het} for deposition freezing (see Eqs. 9–8b in Pruppacher and Klett, 1997), but in order to use the unified formula for both immersion and deposition freezing (Eq. 1), a negative sign is added before Δg^\ddagger (as in Chen et al., 2008). Thus, the fit result for the activation energy in the case of deposition freezing is negative to offset this negative sign.

For the α -PDF model, in the formulation by Chen et al. (2008), the activation energy for the transfer of a water molecule across the water-ice boundary is aerosol-, nucleation-mode- and temperature-dependent and thus should, from a theoretical standpoint, be independent of the contact angle (Zobrist et al., 2007; Hoose et al., 2010). We use the same value for the activation energy as that in the single- α model. The resulting fit parameters from different experiments are listed in Table 2. For the comparison, fit parameters with the single- α model, including CSU106 listed in Table 1, are also given. The experiments were performed over a wide temperature range for Saharan dust sampled in the 2007 International Workshop on Comparing Ice Nucleation Measuring Systems (ICIS-2007; DeMott et al., 2011). These include two experiments of CSU CFDC-1H

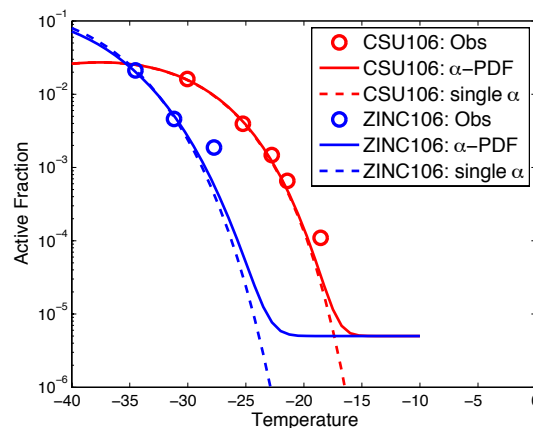


Figure 1. Active fractions determined with CSU106 and ZINC106 (DeMott et al., 2011) are presented as a function of temperature T (indicated by the different color circles). The different lines represent the single- α model and the α -PDF model results fitting the experimentally determined active fractions (parameters in the two models are given in Table 2).

with 106 % and 108 % RH_w (CSU106 and CSU108, respectively) and three experiments conducted with the Zurich Ice Nuclei Chamber (ZINC) at an RH_w of 106 %, 108 % and 110 % (ZINC106, ZINC108 and ZINC110, respectively). It can be seen that the RMSEs with the single- α model are larger in all five experiments than those with the α -PDF model. The reason for this result can be seen in Fig. 1, which shows the observation data from CSU106 and ZINC106 and their fits with the single- α model and the α -PDF model. The α -PDF model reproduces the slow decrease in active fraction with the increase in temperature and shows better agreement with observation data points at warm temperatures ($T > -20^\circ\text{C}$), while the single- α model leads to a steep decrease in active fraction with the increase in temperature and thus results in large errors at warm temperatures. Therefore, larger RMSEs with the single- α model are mainly from its fit at warm temperatures (CSU106 for $T = -18.5^\circ\text{C}$ and ZINC106 for $T = -27.7^\circ\text{C}$). At warmer temperatures, between -10° and -15°C , there are no CFDC observation data to constrain the parameterizations because CFDC can not provide observation data at warm temperatures ($> -15^\circ\text{C}$). However, Niemand et al. (2012) reported the Aerosol Interactions and Dynamics in the Atmosphere (AIDA) cloud chamber measurement of natural dust at temperatures of -13 and -16°C with active fractions of 10^{-4} and 10^{-5} , which agree with our fitted active fractions from the α -PDF model. Saharan natural dust is reported in recent CFDC observations to have onset temperatures ranging from about -10 to -15°C , which is consistent with laboratory observations of various types of surrogate dust (Phillips et al., 2012). Therefore, we apply a cutoff of 0 for the active fractions at temperatures larger than -10°C for two contact angle distributions.

Table 1. Parameters for the ice nucleation parameterization in the single contact angle (α) model. In the table, DeMott et al. (2011) and Koehler et al. (2010) represent Saharan dust. $\Delta g^\#$ is the activation energy; $f_{i,\max,x}$ is the maximum ice nucleating fraction.

Aerosol	Reference	Nucleation mode	α ($^\circ$)	$\Delta g^\#$ (10^{-20} J)	$f_{i,\max,x}$
Soot	DeMott (1990)	Immersion	48.0	14.15	0.01
Dust	DeMott et al. (2011)	Immersion	46.0	14.75	1
Soot	Möhler et al. (2005)	Deposition	28.0	-20	0.01
Dust	Koehler et al. (2010)	Deposition	20.0	-0.81	1

Table 2. Fit parameters obtained for the two models for immersion freezing by dust. The root mean square errors (RMSEs) between the fit curves and the data are given. In the table, μ is the mean contact angle; σ is the standard deviation.

Model	Parameter/RMSE	CSU106	CSU108	ZINC106	ZINC108	ZINC110
Single- α	α ($^\circ$)	46.0	47.0	61.0	61.0	59.0
	$\Delta g^\#$ (10^{-20} J)	14.75	14.4	13.5	13.45	13.65
	RMSE	0.029	0.236	0.087	0.0983	0.147
α -PDF	μ ($^\circ$)	46.0	47.0	62.0	61.0	59.0
	σ	0.01	0.01	0.04	0.01	0.02
	RMSE	0.01	0.225	0.08	0.07	0.08

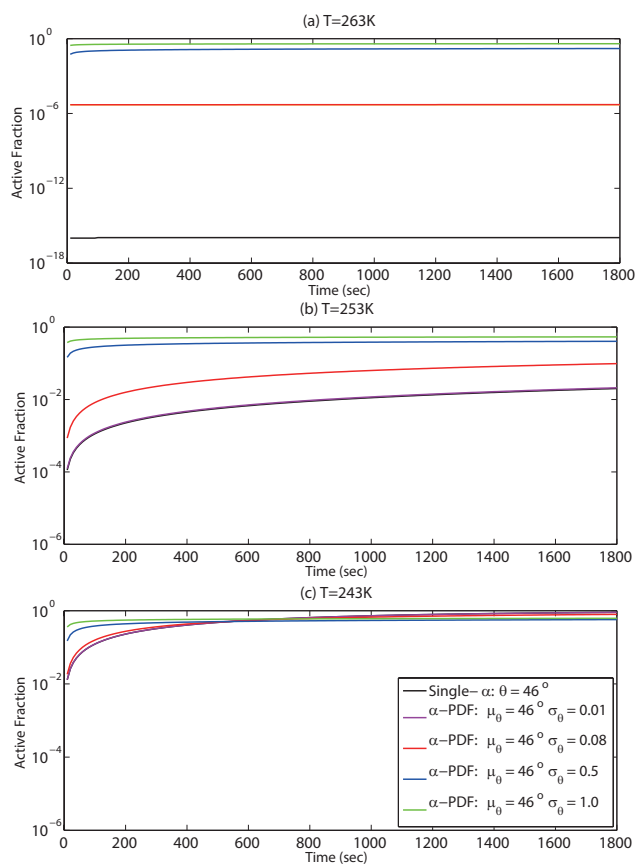


Figure 2. Calculated change in the active fraction with time at different temperatures for 300 nm monodisperse particles and for different contact angle distributions.

3.4 Sensitivity tests for time dependence

We perform sensitivity tests to check whether it is appropriate to use a classical-theory-based parameterization with a crude time step of 30 min in the CAM5 model. Figure 2 shows the active fraction with different contact angle distributions as a function of integration time at different temperatures. It can be seen that, at $T = 263$ K, the active fractions in all contact angle distributions are almost constant with time, indicating very weak dependence of the active fraction on time at warm temperatures (the active fractions in the α -PDF models with $\sigma = 0.01$ and $\sigma = 0.08$ are about 0.499×10^{-5} and 0.516×10^{-5} , respectively, so these two lines overlap). At $T = 253$ K and $T = 243$ K, the active fractions in the single- α model and the α -PDF models with $\sigma = 0.01$ and 0.08 increase with time (the α -PDF model with $\sigma = 0.01$ is very similar to the single- α model), but the active fraction in the α -PDF model with $\sigma = 0.08$ is a little more insensitive to time than that in the single- α model. With increasing standard deviation in the α -PDF model, the active fractions become more weakly dependent on time, the weakest time dependence having $\sigma = 1.0$. As the single- α model can be thought of as the special α -PDF model with $\sigma = 0$ and as increasing the standard deviation reduces the time dependence, we can conclude that the single- α model has a stronger time dependence than the α -PDF model, which is consistent with Welti et al. (2012). Although the single- α model has a stronger time dependence, if we use the following diagnostics, originally developed by Ervens and Feingold (2013), to determine in detail the sensitivity of the active fraction to time, we will find the active fraction in the

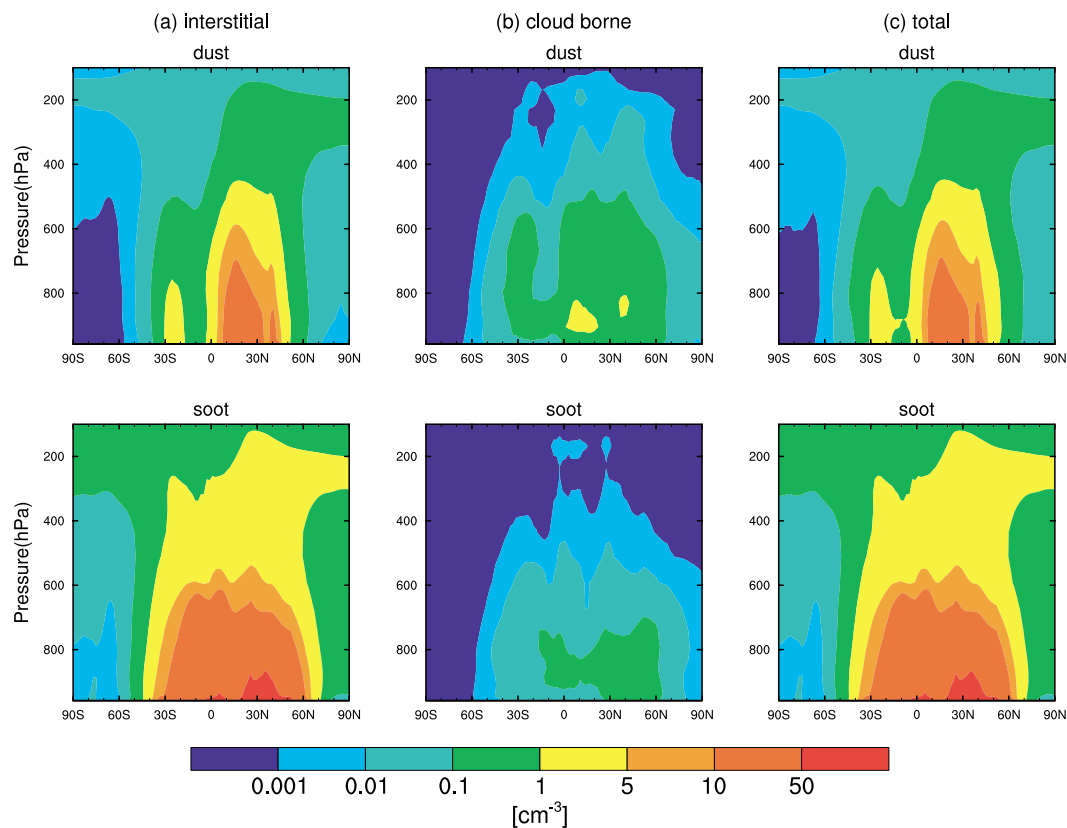


Figure 3. Zonal and annual mean number concentrations (cm^{-3}) of (a) interstitial, (b) cloud-borne and (c) total mineral dust (upper) and soot particles (lower).

single- α model is still only weakly dependent on time.

$$S(X) = \frac{\partial P}{\partial \ln X}, \quad (6)$$

where P is the active fraction and X can be any of the parameters temperature, particle size, contact angle or time (t). At $T = 253$ K, $S(t)$ is 0.0038 from $t = 10$ s ($P = 0.00011$) to $t = 1800$ s ($P = 0.02$). At $T = 243$ K, $S(t)$ is 0.172 from $t = 10$ s ($P = 0.013$) to $t = 1800$ s ($P = 0.9044$). The very small values of $S(t)$ are consistent with the results in Ervens and Feingold (2013). Ervens and Feingold (2013) performed many sensitivity tests to investigate the relative importance of temperature, particle size, contact angle and time for classical nucleation theory. They used Eq. (6) to explore the sensitivity of the active fraction to the above four parameters. As seen in Fig. 1a to d of their paper, they found, from a comparison of $S(X)$, that P is the least sensitive to time of the four parameters. Ervens and Feingold (2013) concluded that a change in T of ~ 1 K has a similar impact on P as θ (contact angle) changes of $\Delta\theta = 2^\circ$, whereas a similar change is only caused by an increase in D_{IN} (particle diameter) by 1 order of magnitude or in t (time) by 3 orders of magnitude. They hence suggested that it seemed feasible to develop more physically (CNT) based relationships instead of the empirically based relationships in large-scale models. Therefore,

the overestimate of the frozen fraction due to a crude time step of 30 min is negligible compared to the uncertainties in temperature and mean contact angle.

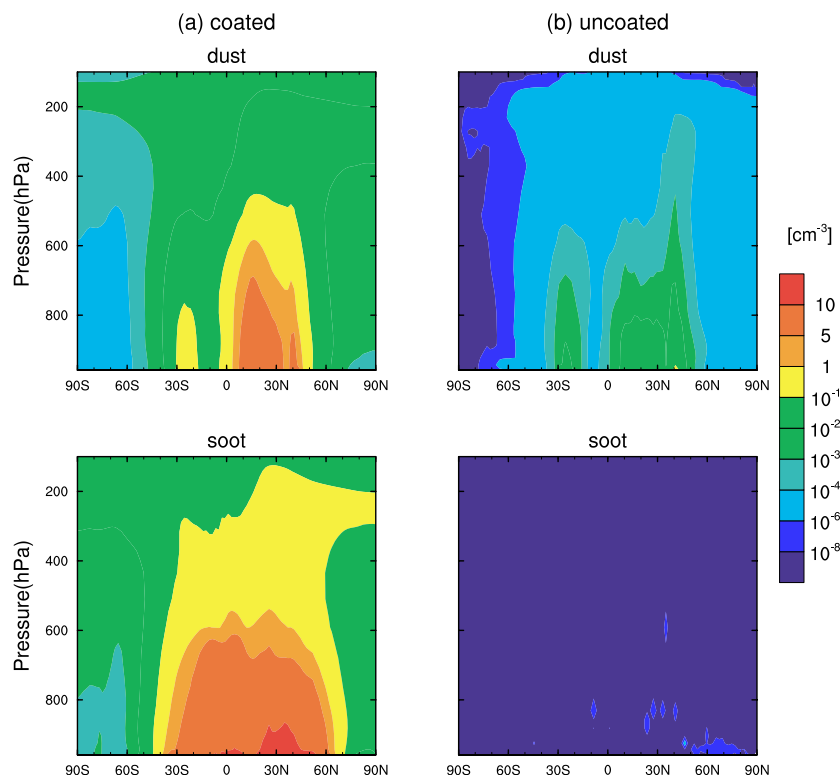
4 Results

A control experiment (CTL) with the default freezing parameterization in CAM5 (Meyers et al., 1992), an experiment based on the CNT in Hoose et al. (2010) (single- α), an experiment with the new α -PDF model as described above and several sensitivity experiments with the α -PDF model have been carried out (see Table 3). The sensitivity experiments are designed to explore the sensitivities of model simulations to the mean contact angle and standard deviation in the α -PDF model. The mean contact angle is changed by $\pm 15^\circ$ (in order to include 61° , which is the fit result from the ZINC measurements), and standard deviation increased by four and eight times in these sensitivity experiments.

All these simulations are run for 6 yr with the model configuration of $1.9^\circ \times 2.5^\circ$ and 30 levels, using prescribed sea surface temperatures (SSTs) and sea ice extent. The aerosol input uses the online aerosol model MAM3. The last 5 yr of results are used in the analysis.

Table 3. Simulation descriptions.

Simulation	Description
CTL	CAM5 with the default heterogeneous ice nucleation parameterization (Meyers et al., 1992)
CNT	As in CTL, but with the classical nucleation theory based on Hoose et al. (2010), using new fitting parameters in Table 1 (e.g., for immersion freezing on dust: $\alpha = 46^\circ$, $\Delta g^\# (10^{-20} \text{ J}) = 14.75$)
PDF	As in CTL, but with the CNT improved by introducing α -PDF model in immersion freezing on dust ($\mu = 46^\circ$, $\sigma = 0.01$)
MU1	As in PDF, but with $\mu = 31^\circ$, $\sigma = 0.01$
MU2	As in PDF, but with $\mu = 61^\circ$, $\sigma = 0.01$
SD1	As in PDF but with $\mu = 46^\circ$, $\sigma = 0.04$ (4σ)
SD2	As in PDF but with $\mu = 46^\circ$, $\sigma = 0.08$ (8σ)

**Figure 4.** Zonal and annual mean number concentrations of (a) interstitial coated and (b) interstitial uncoated mineral dust (upper) and soot particles (lower).

4.1 Particle number concentrations

The zonal and annual mean number concentrations of interstitial, cloud-borne and total (interstitial plus cloud-borne) mineral dust and soot particles are shown in Fig. 3. As is shown in Fig. 3, interstitial dust and soot number concentrations are about 1 order of magnitude larger than those of cloud-borne ones. In cloud-borne aerosols, there are more dust particles than soot particles, which is an important point in explaining the dominant role of dust in heterogeneous freezing compared to soot. The maximum number concentration of interstitial soot, internally mixed in the accumula-

tion mode, is the near-surface layer in the Northern Hemisphere (NH), exceeding 50 cm^{-3} in the zonal mean. Interstitial mineral dust particles in the accumulation and coarse mode reach $10\text{--}50 \text{ cm}^{-3}$ in the subtropics and at the surface of the NH ($\sim 30^\circ \text{ N}$). Interstitial mineral dust and soot are uplifted from their source regions to the middle and upper troposphere and transported to the Arctic in the upper troposphere (Liu et al., 2012b). The total number concentrations of these two species are mainly derived from their interstitial particles (i.e., their cloud-borne particles have negligible contributions to the total number concentrations). As noted

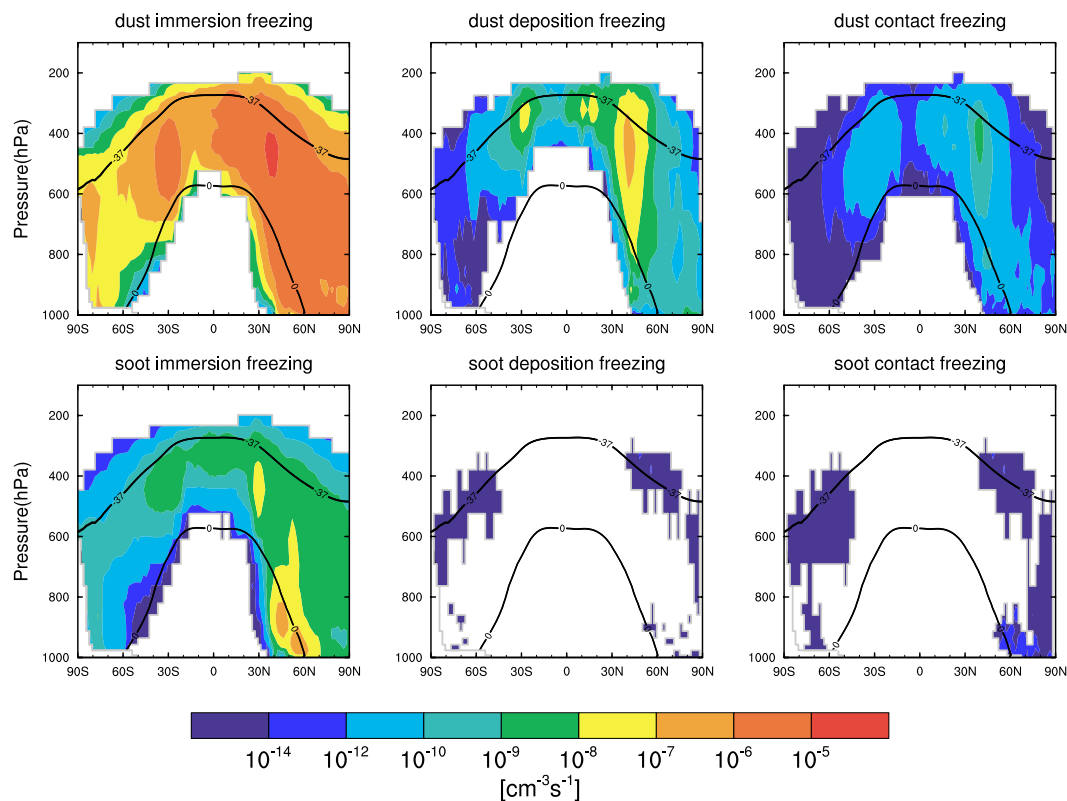


Figure 5. Zonal and annual mean immersion, deposition and contact freezing rates in the PDF simulation. Isotherms of 0 °C and −37 °C are plotted.

above, cloud-borne aerosols are used as an input for immersion freezing, while interstitial aerosols (only the uncoated portion showed in Fig. 4) are used as an input for deposition and contact freezing (see next paragraph for definitions of coated and uncoated portion). Compared to Hoose et al. (2010), the total number concentration of soot is 1 order of magnitude lower in CAM5, which can be attributed to the different size distributions used for soot in two models (CAM5 and CAM3-Oslo). In the CAM3-Oslo model, soot is emitted into the nucleation (initial diameter: 0.024 μm), the Aitken (initial diameter: 0.08 μm) and the accumulation (initial diameter: 0.2 μm) modes (Seland et al., 2008). Its number concentration is dominated by uncoated nucleation and Aitken-mode particles, which contribute to the higher number concentration, while in CAM5 soot is emitted in the accumulation mode with a larger emission size (0.08 μm in diameter). Dust number concentrations in CAM5 are mainly from the accumulation mode, with the diameter range of 0.1–1.0 μm , while coarse-mode number concentration is 1 order of magnitude lower (Liu et al., 2012a). A similar ratio between accumulation and coarse-mode dust is also found in CAM3-Oslo.

The interstitial mineral dust and soot particles are further divided into two categories: coated and uncoated particles. Their number concentrations are derived from the coated

fraction f_{coated} , which is calculated by distributing the soluble mass (sulfate and organic) over the soot and dust cores in the internally mixed modes, requiring a minimum coverage of one monolayer. Suppression of heterogeneous ice nucleation is dependent on coating thickness or the fractional soluble mass coverage. Generally we assume that, if a potential IN is covered by more than one monolayer, its heterogeneous nucleation behavior in the deposition and contact modes will be suppressed completely due to a shift to the higher-onset relative humidity with respect to ice, RH_i , and to the colder onset temperature (Hoose et al., 2010; Möhler et al., 2008). Therefore, only uncoated particles will participate in ice nucleation. The number concentrations of coated and uncoated interstitial aerosol particles are shown in Fig. 4. It can be seen that with the criteria of one monolayer coating by soluble aerosol species the uncoated dust number concentration is several orders of magnitude lower than that of coated dust particles. Compared to dust, nearly all the soot particles are coated (the concentration of the uncoated soot particles is smaller than 10^{-6} cm^{-3}). This is because soot cores have smaller sizes than dust cores and soot is directly emitted into the accumulation mode in MAM3. If soot is directly emitted into the primary carbon mode (e.g., MAM 4 modes (MAM4) or MAM 7 modes (MAM7)), which is the insoluble mode, there should be much more uncoated soot

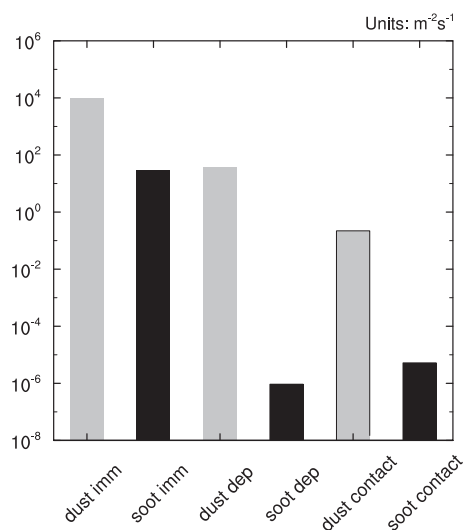


Figure 6. Global and annual mean vertically integrated nucleation rates in the PDF simulation.

particles, especially with slow aging of the primary carbon mode (not shown in this paper). However, as compared to dust, soot is a much less efficient IN, and immersion freezing is the dominant process (see Sect. 4.2). Therefore, it will not have large effects on the total nucleated ice number concentrations even using MAM4 or MAM7.

4.2 Ice nucleation rates

The zonal and annual mean rates of immersion, deposition and contact freezing by dust and soot in the PDF simulation are shown in Fig. 5 ($\Delta N_i/\Delta t$; here ΔN_i is the ice crystal number concentration change predicted only from immersion, deposition and contact freezing over one model time step Δt (30 min); note that it is different from J_{het}). It can be seen that immersion freezing by dust is the dominant ice nucleation mechanism, which is consistent with Hoose et al. (2010), followed by soot immersion, dust deposition and dust contact freezing. Recent observations (de Boer et al., 2011) also indicated that immersion freezing may be the dominant freezing mechanism in mixed-phase clouds when compared to other freezing modes (deposition freezing and contact freezing). This was concluded from the observation that liquid droplets occurred prior to ice formation in mixed-phase clouds, a situation which was also detected by Ansmann et al. (2008). A recent laboratory study by Bunker et al. (2012) found that hundreds of collisions of mineral dust particles with a supercooled droplet are needed to initiate contact freezing. Thus, contact freezing might not be a dominant ice formation pathway in mixed-phase clouds. The other two nucleation modes by soot (i.e., soot deposition and soot contact) are nearly negligible, because the number concentration of uncoated interstitial soot particles is very small (see Fig. 4). In general, the ice nucleation rates peak

over the regions where dust and soot particles are emitted. It should be noted here that freezing rates appear larger than 0 at $T > 0^\circ\text{C}$ and $T < -37^\circ\text{C}$; this is due to zonal and annual averaging. The vertically integrated and globally averaged nucleation rates in the PDF simulation are shown in Fig. 6. The relative roles of all these rates in mixed-phase clouds can be seen more clearly. The freezing rates by dust are similar to those of Hoose et al. (2010). However, the freezing rates by soot are much smaller because of the large differences in the simulated soot number concentrations between the two models (CAM5 and CAM-Oslo) as well as because of the internal mixture of soot in the accumulation mode assumed in CAM5 (Sect. 4.1), which leads to smaller ice nucleation rates in CAM5. In CAM-Oslo, a larger fraction of the soot particles are uncoated and can thus contribute to deposition and contact nucleation; we do not consider this realistic, in particular as these two processes are not observed at warm subzero temperatures in laboratory experiments.

For comparison, the immersion freezing rates by dust simulated by the single- α (CNT) and α -PDF (PDF) models are shown in Fig. 7. We can see that, compared to the single- α model, the major increases in the freezing rates in the α -PDF model are located at low altitudes (with warm temperatures), which is attributed to the PDF distribution of contact angles in the α -PDF model. It means that particles with smaller contact angles in the α -PDF model can nucleate at warm temperatures, whereas the particles with the same contact angles in the single- α model can not nucleate.

4.3 Occurrence frequency of ice nucleation modes

In order to count the different ice nucleation events, we follow the same method as that in Liu et al. (2012b), which counts the homogeneous ice nucleation and heterogeneous ice nucleation events in cirrus clouds when there are new nucleated ice number concentrations from these two ice nucleation modes. Therefore, in this study, we count an ice nucleation event only when the freezing rate ($\Delta N_i/\Delta t$) from one ice nucleation mode is larger than 0. The occurrence frequency of immersion freezing, deposition nucleation and contact nucleation as a function of temperature sampled every 3 h from the PDF simulation and the frequency of immersion freezing from the CNT simulation are shown in Fig. 8. All the data in each temperature bin (2 K) are shown, with the whiskers indicating the 5th and 95th percentiles and with the boxes indicating the 25th and 75th percentiles. The occurrence frequencies for a period of 5 yr (every 3 hr data) are output between -90°S and 90°N and from 1000 hPa to 500 hPa. It can be seen clearly that the frequency of immersion freezing is higher than that of contact nucleation and deposition nucleation. At warm temperatures ($T > 257\text{K}$), the frequency of deposition nucleation decreases rapidly with the increase in temperature, resulting in one order of magnitude smaller than that of contact nucleation. The frequency

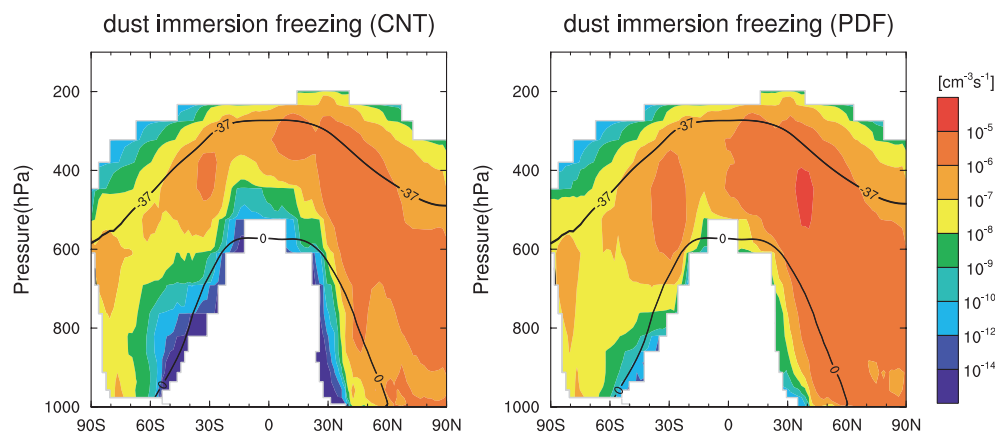


Figure 7. Zonal and annual mean immersion freezing rates in the CNT and PDF simulations. Isotherms of 0 °C and −37 °C are plotted.

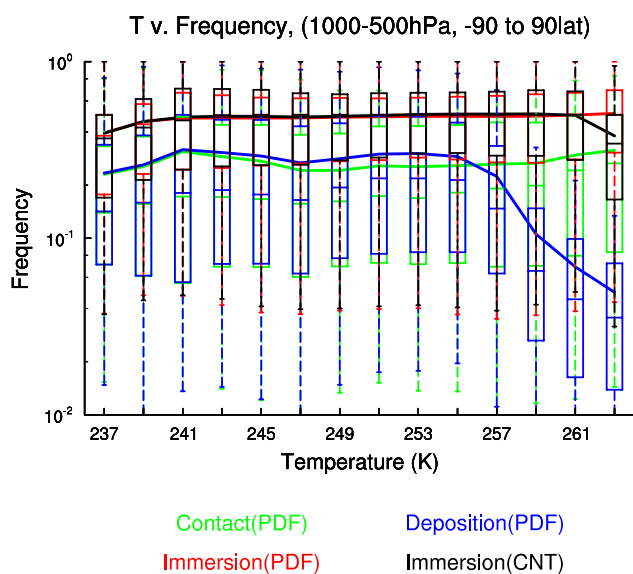


Figure 8. Simulated frequency of immersion freezing (red), deposition nucleation (blue) and contact nucleation (green) in the PDF simulation and immersion freezing (black) in the CNT simulation as a function of temperature sampled every 3 h. The whiskers represent the 5th and 95th percentiles, and the boxes represent the 25th and 75th percentiles and the median.

of immersion freezing in the PDF simulation at $T > 261$ K is higher than that in the CNT simulation.

Figure 9 shows the zonal and annual mean frequency distribution of immersion freezing, deposition nucleation and contact nucleation. The pattern of immersion freezing is different from the two other modes. There are two maximum centers located in the polar regions. The deposition and contact nucleation peak over the source regions at 30–60° N and 20–40° S. This is because dust and soot near the source regions are uncoated, leading to the occurrence of deposition and contact nucleation. When these particles age and are coated in the process of being uplifted and transported to po-

lar regions, deposition and contact nucleation become even less important and, conversely, immersion freezing dominates. The frequency of immersion freezing after introducing the α -PDF model (PDF) compared to the single- α model (CNT) increases a little at low altitudes (with warm temperatures).

4.4 Sensitivity tests with the α -PDF model

Figure 10 shows the effects of changes in the uncertain parameters in the α -PDF model on active fraction with temperature. Figure 10a shows the impact of the mean contact angle. It is obvious that, with the decrease in the mean contact angle, the active fraction increases, making the curve shift upwards. However, the temperature range in which ice fraction rapidly increases does not become broader, indicating that changes in the mean contact angle do not change the slope of variations in active fraction with temperature much. Instead, in Fig. 10b, the temperature dependence of the active fraction changes with the change in the standard deviation. With the increase in standard deviation, a broader distribution of contact angles will be allocated to aerosol particles. Since the different contact angle on each particle results in a different freezing temperature for each particle, the temperature range in which droplets freeze becomes broader. For example, for $\sigma = 0.01$, droplets freeze within a narrow temperature interval of about 10 °C, while for $\sigma = 0.08$, freezing occurs over a temperature range of about 18 °C. The change in the active fraction with temperature (Fig. 10b) becomes smoother with an increase in the standard deviation, which indicates the “recovery” of singular behavior (Niedermeier et al., 2011, 2014; Welti et al., 2012) and a weakening of the time dependence of stochastic behavior (see Fig. 2 for the change in time dependence with an increase in the standard deviation). Although the magnitude of changes in active fraction due to the change in the standard deviation is much smaller than that due to the mean contact angle at a given temperature, increasing the standard deviation results in the transition of the

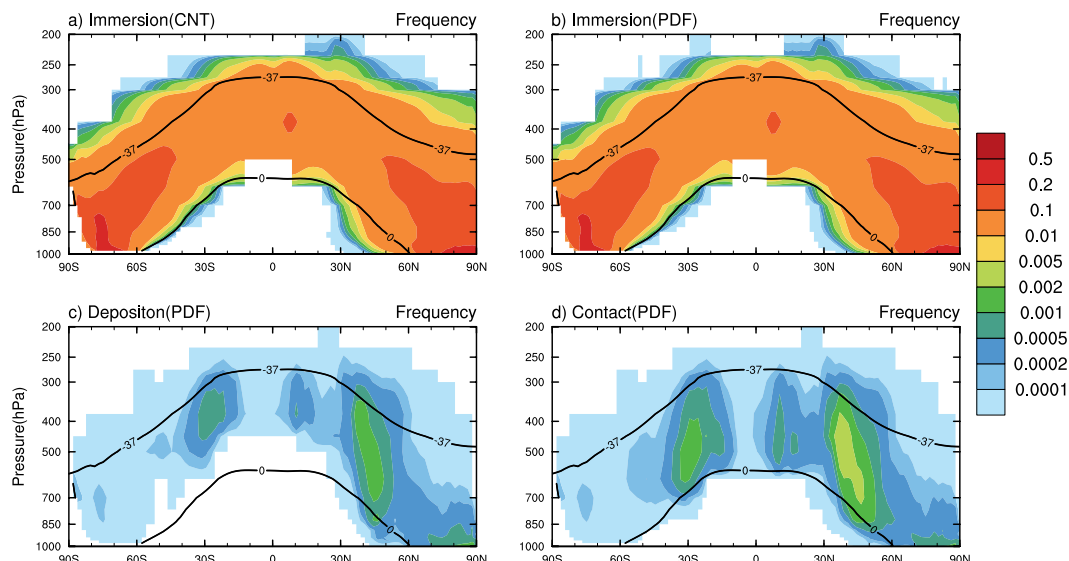


Figure 9. Zonal and annual mean distribution of the occurrence frequency of (a) immersion mode in the CNT simulation and (b) immersion, (c) deposition and (d) contact freezing modes in the PDF simulation. Isotherms of 0 °C and –37 °C are plotted.

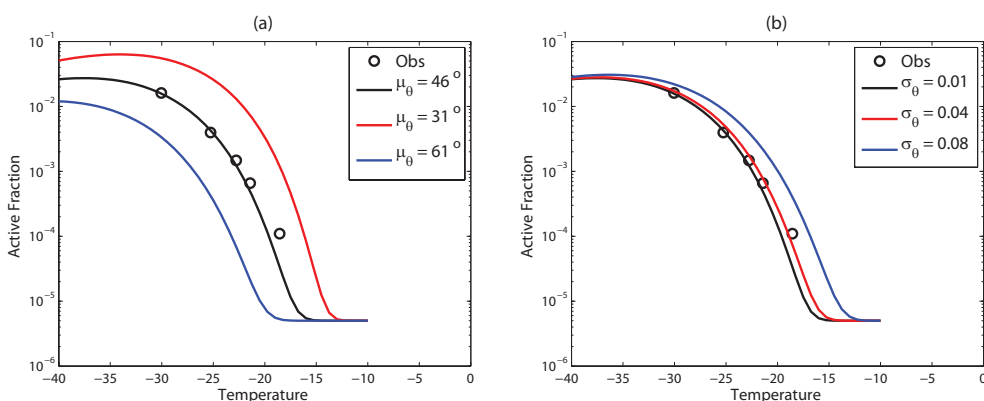


Figure 10. Active fraction as a function of temperature for the α -PDF model settings. Observation data are from CSU106 and the black solid line is its fit curve. The red and blue solid lines are sensitivity tests to (a) mean contact angle and (b) standard deviation.

freezing behavior from stochastic behavior to singular behavior (Niedermeier et al., 2011, 2013). Some variations in cloud properties with the changes in these uncertain parameters in the α -PDF model will be shown in Sect. 4.6.

4.5 Comparison of IN Concentrations with observations

Currently the most frequently used instrument for detecting IN concentrations in the atmosphere is the CFDC (Rogers et al., 2001), which allows interstitial aerosol particles to enter through an inlet and be exposed to a specific temperature and/or humidity in the chamber. Then, the number concentration of ice crystals nucleated in the chamber after a residence time of 5–20 s is counted. We calculate modeled IN concentrations and compare them with CFDC observa-

tions. The calculation uses modeled interstitial aerosol concentrations which are sampled at the same locations and pressures as observations and with the same processing temperatures as operated in the CFDC. In the same way, the relative humidity is assumed to be equal to the processing conditions in the instrument. It is assumed in our calculations that 100 % of the relative humidity with respect to water (RH_w) is used for immersion freezing and 98 % RH_w for deposition freezing. Thus, immersion/condensation and deposition nucleation modes are taken into account, which is consistent with the observed dominant ice nucleation modes in the CFDC. The reason that the contact nucleation mode is not considered is that the residence time in the CFDC is short, and thus its technique can not directly assess whether aerosol particles are active as contact freezing nuclei (DeMott et al., 2010).

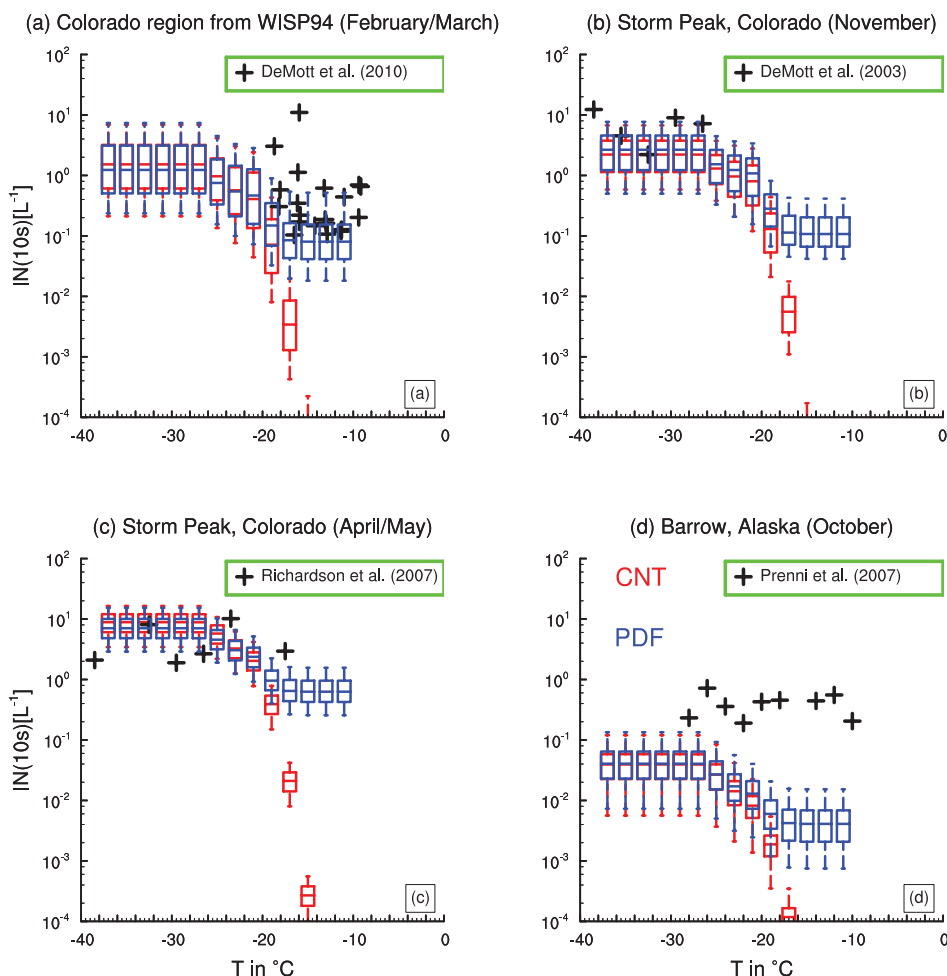


Figure 11. IN(10s) concentrations for specified temperature, selected at the grid points including the measurement locations and at the same pressure level as field observations in the CNT simulation (red boxes and whiskers) and in the PDF simulation (blue boxes and whiskers). The whiskers represent the 5th and 95th percentiles, and the boxes represent the 25th and 75th percentiles and the median. The black crosses indicate CFDC IN measurements.

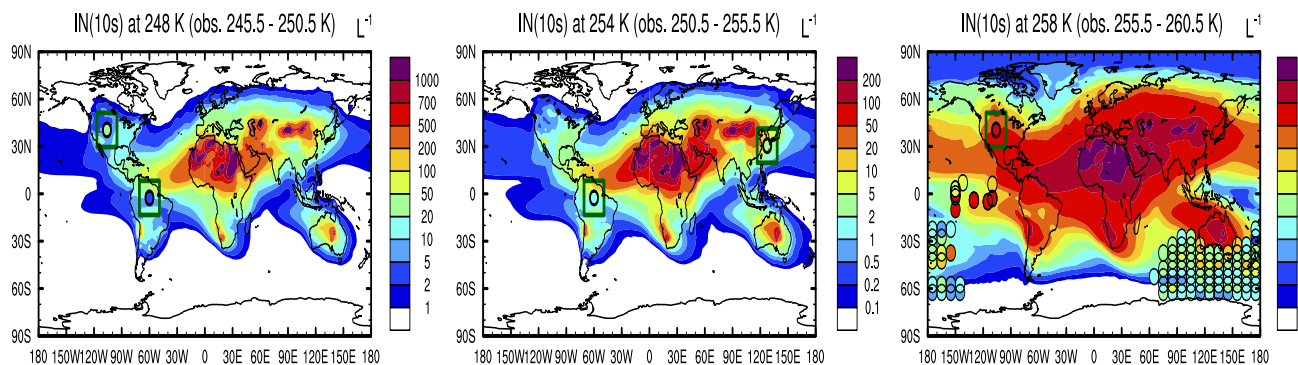


Figure 12. Spatial comparison of IN(10s) concentration with field data. IN(10s) concentrations are sampled for three specific temperatures, which fall into the same range of observed temperatures as chosen for measurements at the near-surface layer. The field IN measurements are indicated by colored circles (DeMott et al. (2010) in the central USA; Rosinski et al. (1987) in the central Pacific; Rosinski et al. (1995) in the East China Sea; Bigg et al. (1973) to the south of Australia). Field IN measurements in the East China Sea, Brazil and the central USA are highlighted by dark green rectangles to show them more clearly.

Both the single- α and α -PDF models are time-dependent, and CFDC has a residence time of approximately 10 s, so we define the modeled IN number concentration (hereafter termed “model IN(10s)”) as a 10 s integral over the freezing rate ($\Delta N_i/\Delta t$) in order to provide direct comparability to the observations, following Hoose et al. (2010). Figure 11 shows the model IN(10s) concentrations in two simulations (CNT and PDF), which are diagnosed based on interstitial aerosol concentrations from the simulations at the measurement locations and are diagnosed at the same pressure level as field observations. The magnitude of model IN(10s) concentrations simulated by CNT and PDF is similar to observations except in the case of Barrow, Alaska (some data points which are clearly below the acceptable minimum detection limit of CFDC are removed). At warmer temperatures ($T > -20^\circ\text{C}$) model IN(10s) concentrations simulated by the PDF simulation during the Winter Icing in Storms Project in 1994 (WISP94) in the Colorado region in February and March (Fig. 11a) and at Storm Peak in April and May (Fig. 11c) agree better with observations than the concentrations simulated by CNT which are several orders of magnitude smaller than observations. The modeled weak temperature dependence at $T > -20^\circ\text{C}$ in the Colorado region (Fig. 11a) in the PDF simulation is confirmed by observations, where there is an indication of the trend being flatter (the observation data in Lüönd et al. (2010) also shows this trend at warm temperatures). By contrast, when the temperature is warmer than -20°C , the IN(10s) concentrations simulated by the CNT simulation reduce rapidly, resulting in a discrepancy of several orders of magnitude with observations (see Fig. 11a and c). The temperature variation of model IN(10s) concentrations in the CNT and PDF simulations becomes flat at $T < -25^\circ\text{C}$ at Storm Peak (Fig. 11b and c), which is consistent with the observations. The model IN(10s) concentrations at Barrow, Alaska (Fig. 11d), in the CNT and PDF simulations are both 1 or 2 orders of magnitude smaller than observations. Due to good agreement of IN(10s) concentrations with observations (see Fig. 11a–c) and a confirmed relationship between IN concentrations and aerosol number concentrations with a diameter larger than $0.5\ \mu\text{m}$ for all grid points (see Fig. 12 for details), we may deduce that the simulated aerosol number concentrations with a diameter larger than $0.5\ \mu\text{m}$ in these locations (i.e., Fig. 11a–c) should be in agreement with observations, and the large underestimates of IN(10s) concentrations in Barrow, Alaska, are due to the fact that the simulated number concentrations of aerosol particles (e.g., soot) in the Arctic are 1 or 2 orders of magnitude smaller than observations (Wang et al., 2011; Liu et al., 2012a).

For a more detailed comparison for warm temperature regions, spatial distributions of model IN(10s) concentrations from the simulation PDF are shown in Fig. 12 with some field measurements of IN concentrations around the globe (DeMott et al. (2010), central USA, $239\ \text{K} < T < 246\ \text{K}$ and $241\ \text{K} < T < 258\ \text{K}$; Rosinski et al. (1987), the central Pa-

cific, $254\ \text{K} < T < 260.5\ \text{K}$; Rosinski et al. (1995), East China Sea, $T = 253\ \text{K}$; Bigg et al. (1973), the south of Australia, $T = 258\ \text{K}$). As there is only one single field campaign in the East China Sea, Brazil and central USA regions, (i.e., only one single circle in each region in Fig. 12) and the regions’ colors are similar to the background colors of modeled IN(10s) concentrations, we utilize dark green rectangles to show them more clearly. The model IN(10s) concentrations are selected for three specific temperatures, which fall into the corresponding range of observed temperatures as specified in each plot. All the field measurements are located at the surface, and thus we also use interstitial aerosol concentrations at the surface as input to diagnose IN concentrations. It can be seen that the model IN(10s) concentrations are in agreement with observations, especially in the East China Sea, Brazil and the central USA. In near-surface air over marine regions, marine biogenic IN (types of marine biogenic particles include marine microorganisms, exopolymer secretions/colloidal aggregates, glassy organic aerosols, crystalline hydrated NaCl and frost flowers), unlike dust IN, are most likely to play a dominant role in determining IN concentrations at high temperatures. Thus over the Southern Ocean at $258\ \text{K}$, especially near the Antarctic coast, the model greatly underestimates IN(10s) concentrations (Burrows et al., 2013). Another region where the model significantly underestimates IN(10s) concentrations at $258\ \text{K}$ is over the Pacific. In the remote marine boundary layer of the equatorial Pacific Ocean, ship-based measurements found that atmospheric IN concentrations were associated with high concentrations of biogenic materials due to ocean upwelling (Rosinski et al., 1987). Therefore, as can be seen from Figs. 11 and 12, the α -PDF model enhances the IN concentrations at warm temperatures and agrees well with observations, which can be attributed to a distribution of contact angles.

Georgii and Kleinjung (1967) found that IN number concentrations correlate well with the number concentration of coarse-mode aerosol particles but not with the total aerosol number concentration, which is dominated by smaller particles. More recent IN measurements with the CFDC obtained similar results (DeMott et al., 2006; DeMott et al., 2010; DeMott et al., 2014). Fig. 13 shows the model IN(10s) concentrations in the CNT and PDF simulations as a function of number concentrations of aerosols with a diameter larger than $0.5\ \mu\text{m}$ (N_{a500}), sampled at $T = -21^\circ\text{C}$ (Fig. 13a and b), which is the temperature used in the observations (DeMott et al., 2006; Georgii and Kleinjung, 1967), and sampled at $T = -27^\circ\text{C}$ (Fig. 13c and d) which is used in DeMott et al. (2014). In CAM5, we sample N_{a500} as follows: the accumulation-mode dust number concentration with a diameter larger than $0.5\ \mu\text{m}$ is calculated with the predicted dust mass mixing ratio of this mode and the prescribed size distribution for transported dust (Zender et al., 2003) (transported dust is in coarse mode with a mass median diameter of $2.524\ \mu\text{m}$, and the standard deviation is 2.0). The dust

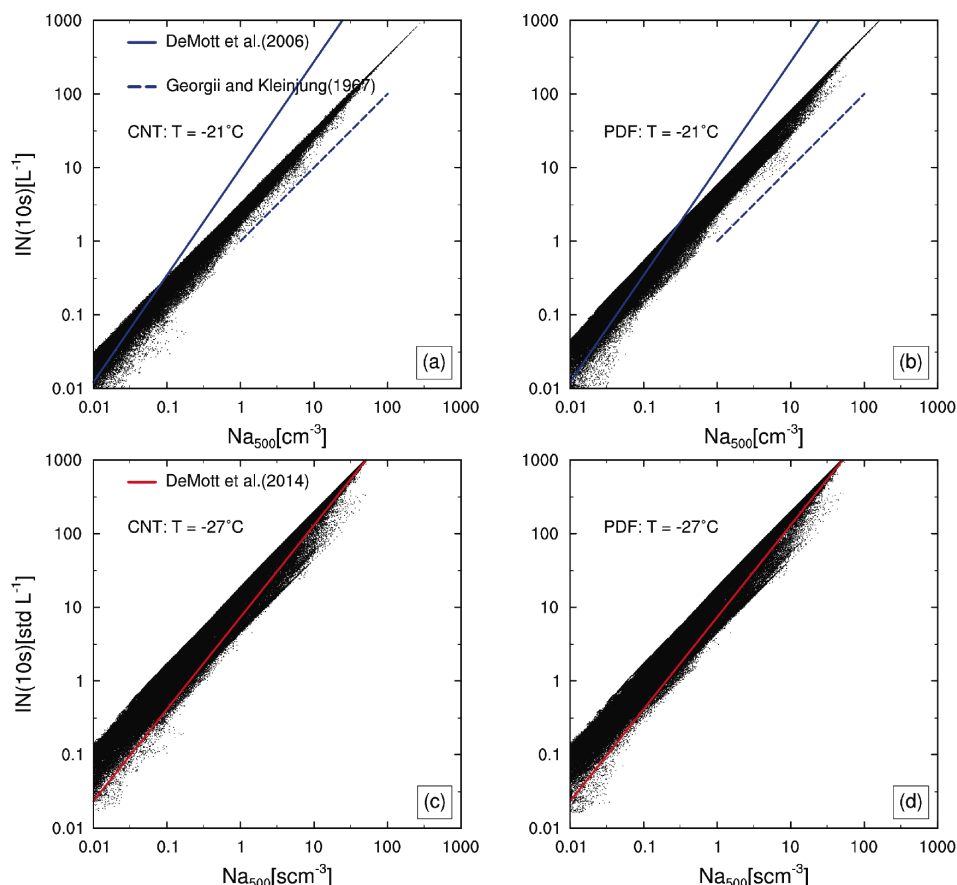


Figure 13. IN(10s) concentrations in the CNT and PDF simulations, displayed as a function of the number concentrations of aerosol particles with a diameter greater than $0.5\ \mu\text{m}$ at $T = -21\ ^\circ\text{C}$ (a and b), which is the observed temperature used in the power-law fit to observations (DeMott et al., 2006 (solid blue line); Georgii and Kleinjung 1967 (dashed blue line)) and at $T = -27\ ^\circ\text{C}$ (c and d), which is used for the parameterization proposed by DeMott et al. (2014) (solid red line).

number concentration in the coarse mode is calculated from the predicted total number concentration in the coarse mode weighted by the mass fraction of dust in this mode. Following this, we use these two dust number concentrations as the Na_{500} . We neglect the contribution of soot (due to its smaller size) and sea salt to Na_{500} . In Fig. 13a and b, for both the CNT and PDF simulations, almost all dots are located in between the two power-law fits by DeMott et al. (2006) and Georgii and Kleinjung (1967). Compared to the CNT simulation, the model IN(10s) concentrations simulated from the PDF simulation shift upwards a little. In order to compare them with DeMott et al. (2014), we convert modeled Na_{500} and IN(10s) to values at standard temperature and pressure conditions ($\text{Na}_{500}[\text{s cm}^{-3}]$ and $\text{IN}(10\text{s})[\text{std L}^{-1}]$), and the results are shown in Fig. 13c and d. Both in the CNT and PDF simulations, the magnitude of the model IN(10s) concentrations is at and around the parameterization proposed by DeMott et al. (2014) (solid red line), thus yielding excellent agreement. The DeMott et al. (2014) parameterization, developed from the DeMott et al. (2010) parameterization to account for additional aerosol compositional dependen-

cies, is exclusively for dust ice nuclei. For atmospheric application, an additional correction factor is introduced to account for the underestimate of the immersion freezing fraction of mineral dust particles for CFDC data. The parameterization reflects the mineral dust data from the Saharan or Asian regions very well and indicates that they can be parameterized as a common particle type for global modeling. Therefore, the atmospheric application of our parameterization based on Saharan dust is successfully confirmed by DeMott et al. (2014).

4.6 Aerosol indirect effect

Table 4 lists the global and annual mean cloud and radiative properties for the present-day simulations and differences in these variables between the present-day and preindustrial simulations. As for the present-day experiments, with the implementation of two stochastic heterogeneous ice nucleation parameterizations, the global mean ice water path (IWP) decreases for the CNT and all the PDF simulations compared to the CTL simulation due to fewer nucleated ice

Table 4. Global annual mean fields for the present-day simulations and differences in these variables between present-day and preindustrial simulations. Variables listed in the table are total cloud cover (TCC, %), low cloud cover (LCC, %), liquid-water path (LWP, g m^{-2}), ice water path (IWP, g m^{-2}), shortwave cloud forcing (SWCF, W m^{-2}), long-wave cloud forcing (LWCF, W m^{-2}), net cloud forcing (CF, W m^{-2}) and integrated column ice number concentration in mixed-phase clouds (ICENUM, 10^3 cm^{-2}).

Run	CTL	CNT	PDF	MU1	MU2	SD1	SD2
TCC	64.0	64.0	63.9	64.0	64.1	64.0	64.0
Δ TCC	0.14	0.42	0.28	0.57	0.59	0.44	0.62
LCC	43.6	43.1	43.1	43.1	43.2	43.1	43.1
Δ LCC	0.32	0.58	0.49	0.68	0.72	0.66	0.72
LWP	44.59	46.41	46.51	46.34	46.72	46.60	46.56
Δ LWP	3.26	3.66	3.80	3.73	3.98	3.96	3.77
IWP	17.78	16.10	16.22	16.28	16.23	16.27	16.24
Δ IWP	0.14	0.16	0.32	0.42	0.34	0.36	0.33
SWCF	-52.00	-52.10	-52.20	-52.17	-52.34	-52.24	-52.25
Δ SWCF	-1.64	-1.82	-1.94	-2.01	-2.08	-2.03	-2.05
LWCF	24.04	23.61	23.65	23.65	23.75	23.69	23.68
Δ LWCF	0.50	0.76	0.82	0.92	0.92	0.81	0.84
CF	-27.96	-28.47	-28.55	-28.52	-28.58	-28.55	-28.56
Δ CF	-1.14	-1.06	-1.13	-1.10	-1.16	-1.22	-1.21
ICENUM	2.863	2.366	2.395	2.407	2.381	2.401	2.389
Δ ICENUM	0.036	0.045	0.074	0.068	0.052	0.069	0.066

crystals in the CNT and PDF simulations. This can be confirmed from the comparison, among different simulations, of the vertically integrated column ice crystal number concentration (ICENUM) in mixed-phase clouds ($-37^\circ\text{C} < T < 0^\circ\text{C}$). The CTL simulation has the largest ICENUM in mixed-phase clouds, which is because Meyers et al. (1992) scheme overestimates the nucleated ice number concentrations (DeMott et al., 2010). As a consequence, the CNT and all the PDF simulations exhibit a larger global mean liquid-water path (LWP) than that in the CTL simulation. This is because fewer ice crystals slow down the Wegener–Bergeron–Findeisen process and thus increase the liquid-water content. The larger (smaller) mean contact angle with the smaller (larger) active fraction in MU1 (MU2) (the PDF sensitivity simulations with only modifying the mean contact angle) results in smaller (larger) ICENUM in mixed-phase clouds.

The LWP and IWP changes between the present day and the preindustrial period in the CTL simulation are 3.26 g m^{-2} and 0.14 g m^{-2} , respectively, while those in the CNT and PDF simulations are larger, especially the IWP change. There may be two reasons that cause the changes in IWP between the present-day and preindustrial simulations with the new parameterizations to be generally larger than those in CTL. One reason is increased dust concentrations (partly due to less efficient wet scavenging) and increased soot concentrations in the PD simulations (the default scheme in CTL doesn't link to aerosols). The other reason may be that soot is taken into account in the new parameterizations, which enlarges the differences between the present-day and preindustrial simulations. Larger changes in IWP and LWP between the present day and the preindustrial period in the

CNT and PDF simulations lead to larger changes in shortwave cloud forcing (SWCF) and long-wave cloud forcing (LWCF). The SWCF change differs by 0.18 W m^{-2} and LWCF change by 0.26 W m^{-2} between the CTL and CNT simulations (0.30 W m^{-2} and 0.32 W m^{-2} between the CTL and PDF simulations, respectively), although the net cloud forcing change differs by less than 0.1 W m^{-2} . The changes in total cloud cover (TCC), low cloud cover (LCC) and integrated column ice crystal number concentration (ICENUM) in the mixed-phase clouds between the present day and the preindustrial period are also larger in the CNT and PDF simulations than those in the CTL simulation.

5 Conclusions

A classical-nucleation-theory-based parameterization of heterogeneous ice nucleation is implemented in CAM5 based on Hoose et al. (2010). In addition, we make further improvements by introducing a probability distribution of contact angles for the freezing process by natural dust. We fit the uncertain parameters of the single- α and the α -PDF models to laboratory data for natural dust and BC (soot). Compared to the single- α model, the α -PDF model shows better agreement with observations at warm temperatures ($T > -20^\circ\text{C}$) by enhancing the IN number concentrations and, further, results in a weaker temperature dependence of IN number concentration. Therefore, more ice crystals can form at low altitudes (with warm temperatures) from the α -PDF model than from the single- α model.

From the sensitivity tests with the α -PDF model, we find that though the change in mean contact does not change

the slope of variations of active fraction with temperature, it can still change the active fraction at a given temperature. When increasing (reducing) the mean contact angle, the active fraction will decrease (increase). Meanwhile, the increase in standard deviation will lead to a change in nucleation behavior from stochastic behavior to singular behavior. Judging by the absolute changes in the active fraction at a given temperature (not by its temperature dependence), the mean contact angle has a larger impact on the active fraction than standard deviation, which is consistent with the cloud-resolving model results by Kulkarni et al. (2012). Immersion freezing by natural dust in both single- α and α -PDF models is the dominant nucleation mechanism in mixed-phase clouds, consistent with Hoose et al. (2010). After implementing the new parameterizations, there are significant boosts to LWP due to the nucleated ice number concentration having been effectively reduced. The new parameterizations also induce more significant aerosol indirect effects than the default parameterization.

Although the heterogeneity of individual particles in the aerosol population has been taken into account in introducing the α -PDF model, the heterogeneity of the surface area of each particle can also influence the freezing behavior. Therefore, other stochastic models considering the heterogeneity of surface area, such as the active site model and the soccer ball model (Niedermeier et al., 2014), should be implemented, and then their behavior should be explored in global models.

Acknowledgements. We would like to thank P. J. DeMott for providing the CFDC data shown in Figs. 10 and 11. This research was supported by the Office of Science of the US Department of Energy (DOE) as part of the Earth System Modeling Program. We would like to acknowledge the use of computational resources (ark:/85065/d7wd3xhc) at the NCAR-Wyoming Supercomputing Center provided by the National Science Foundation and the State of Wyoming, and supported by NCAR's Computational and Information Systems Laboratory. C. Hoose acknowledges funding by the Helmholtz Association through the President's Initiative and Networking Fund and by the Deutsche Forschungsgemeinschaft through project FOR 1525. We would like to thank the anonymous reviewers very much for their helpful suggestions.

Edited by: H. Su

References

Abdul-Razzak, H. and Ghan, S. J.: A parameterization of aerosol activation: 2. Multiple aerosol types, *J. Geophys. Res.-Atmos.*, 105, 6837–6844, doi:10.1029/1999JD901161, 2000.

Ansmann, A., Tesche, M., Althausen, D., Müller, D., Seifert, P., Freudenthaler, V., Heese, B., Wiegner, M., Pisani, G., Knipfertz, P., and Dubovik, O.: Influence of Saharan dust on cloud glaciation in southern Morocco during the Saharan Min-

eral Dust Experiment, *J. Geophys. Res.-Atmos.*, 113, D04210, doi:10.1029/2007JD008785, 2008.

Barahona, D.: On the ice nucleation spectrum, *Atmos. Chem. Phys.*, 12, 3733–3752, doi:10.5194/acp-12-3733-2012, 2012.

Bigg, E. K.: The formation of atmospheric ice crystals by the freezing of droplets, *Q. J. Roy. Meteor. Soc.*, 79, 510–519, doi:10.1002/qj.49707934207, 1953.

Bigg, E. K.: Ice nucleus concentrations in remote areas, *J. Atmos. Sci.*, 30, 1153–1157, doi:10.1175/1520-0469(1973)030<1153:INCIRA>2.0.CO;2, 1973.

Bretherton, C. S. and Park, S.: A new moist turbulence parameterization in the community atmosphere model, *J. Climate*, 22, 3422–3448, doi:10.1175/2008JCLI2556.1, 2009.

Bunker, K. W., China, S., Mazzoleni, C., Kostinski, A., and Cantrell, W.: Measurements of ice nucleation by mineral dusts in the contact mode, *Atmos. Chem. Phys. Discuss.*, 12, 20291–20309, doi:10.5194/acpd-12-20291-2012, 2012.

Burrows, S. M., Hoose, C., Pöschl, U., and Lawrence, M. G.: Ice nuclei in marine air: biogenic particles or dust?, *Atmos. Chem. Phys.*, 13, 245–267, doi:10.5194/acp-13-245-2013, 2013.

Chen, J.-P., Hazra, A., and Levin, Z.: Parameterizing ice nucleation rates using contact angle and activation energy derived from laboratory data, *Atmos. Chem. Phys.*, 8, 7431–7449, doi:10.5194/acp-8-7431-2008, 2008.

Cooper, W. A.: A possible mechanism for contact nucleation, *J. Atmos. Sci.*, 31, 1832–1837, doi:10.1175/1520-0469(1974)031<1832:APMFCN>2.0.CO;2, 1974.

de Boer, G., Morrison, H., Shupe, M. D., and Hildner, R.: Evidence of liquid dependent ice nucleation in high-latitude stratiform clouds from surface remote sensors, *Geophys. Res. Lett.*, 38, L01803, doi:10.1029/2010GL046016, 2011.

DeMott, P. J.: An exploratory study of ice nucleation by soot aerosols, *J. Appl. Meteorol.*, 29, 1072–1079, doi:10.1175/1520-0450(1990)029<1072:AESOIN>2.0.CO;2, 1990.

DeMott, P. J., Cziczo, D. J., Prenni, A. J., Murphy, D. M., Kreidenweis, S. M., Thomson, D. S., Borys, R., and Rogers, D. C.: Measurements of the concentration and composition of nuclei for cirrus formation, *P. Natl. Acad. Sci. USA*, 100, 14655–14660, doi:10.1073/pnas.2532677100, 2003.

DeMott, P. J., Prenni, A. J., Richardson, M. S., Kreidenweis, S. M., Twohy, C. H., and Rogers, D. C.: Ice nuclei variability, relation to ambient aerosol properties, and impacts on mixed-phase clouds. Preprints, 12th Conf. on Cloud Physics, Madison, WI, Amer. Meteor. Soc., 2.1, 10 July 2006, available at: http://ams.confex.com/ams/Madison2006/techprogram/paper_113242.htm, 2006.

DeMott, P. J., Prenni, A. J., Liu, X., Kreidenweis, S. M., Petters, M. D., Twohy, C. H., Richardson, M. S., Eidhammer, T., and Rogers, D. C.: Predicting global atmospheric ice nuclei distributions and their impacts on climate, *P. Natl. Acad. Sci. USA*, 107, 11217–11222, doi:10.1073/pnas.0910818107, 2010.

DeMott, P. J., Möhler, O., Stetzer, O., Vali, G., Levin, Z., Petters, M. D., Murakami, M., Leisner, T., Bundke, U., Klein, H., Kanji, Z. A., Cotton, R., Jones, H., Benz, S., Brinkmann, M., Rzesanke, D., Saathoff, H., Nicolet, M., Saito, A., Nillius, B., Bingemer, H., Abbatt, J., Ardon, K., Ganor, E., Georgakopoulos, D. G., and Saunders, C.: Resurgence in ice nuclei measurement research, *B. Am. Meteorol. Soc.*, 92, 1623–1635, doi:10.1175/2011BAMS3119.1, 2011.

- DeMott, P. J., Prenni, A. J., McMeeking, G. R., Sullivan, R. C., Petters, M. D., Tobo, Y., Niemand, M., Möhler, O., Snider, J. R., Wang, Z., and Kreidenweis, S. M.: Integrating laboratory and field data to quantify the immersion freezing ice nucleation activity of mineral dust particles, *Atmos. Chem. Phys. Discuss.*, 14, 17359–17400, doi:10.5194/acpd-14-17359-2014, 2014.
- Diehl, K. and Würzler, S.: Heterogeneous drop freezing in the immersion mode: model calculations considering soluble and insoluble particles in the drops, *J. Atmos. Sci.*, 61, 2063–2072, doi:10.1175/1520-0469(2004)061<2063:HDFIT>2.0.CO;2, 2004.
- Ervens, B. and Feingold, G.: Sensitivities of immersion freezing: Reconciling classical nucleation theory and deterministic expressions, *Geophys. Res. Lett.*, 40, 3320–3324, doi:10.1002/grl.50580, 2013.
- Georgii, H. and Kleinjung, E.: Relations between the chemical composition of atmospheric aerosol particles and the concentration of natural ice nuclei, *J. Rech. Atmos.*, 3, 145–156, 1967.
- Gottelman, A., Morrison, H., and Ghan, S. J.: A new two-moment bulk stratiform cloud microphysics scheme in the Community Atmosphere Model, Version 3 (CAM3). Part II: Single-column and global results, *J. Climate*, 21, 3660–3679, doi:10.1175/2008JCLI2116.1, 2008.
- Gottelman, A., Liu, X., Ghan, S. J., Morrison, H., Park, S., Conley, A. J., Klein, S. A., Boyle, J., Mitchell, D. L., and Li, J. L. F.: Global simulations of ice nucleation and ice supersaturation with an improved cloud scheme in the Community Atmosphere Model, *J. Geophys. Res.-Atmos.*, 115, D18216, doi:10.1029/2009JD013797, 2010.
- Hoose, C., Lohmann, U., Erdin, R., and Tegen, I.: The global influence of dust mineralogical composition on heterogeneous ice nucleation in mixed-phase clouds, *Environ. Res. Lett.*, 3, 025003, doi:10.1088/1748-9326/3/2/025003, 2008.
- Hoose, C., Kristjánsson, J. E., Chen, J.-P., and Hazra, A.: A classical-theory-based parameterization of heterogeneous ice nucleation by mineral dust, soot, and biological particles in a global climate model, *J. Atmos. Sci.*, 67, 2483–2503, doi:10.1175/2010JAS3425.1, 2010.
- Hoose, C. and Möhler, O.: Heterogeneous ice nucleation on atmospheric aerosols: a review of results from laboratory experiments, *Atmos. Chem. Phys.*, 12, 9817–9854, doi:10.5194/acp-12-9817-2012, 2012.
- Iacono, M. J., Delamere, J. S., Mlawer, E. J., Shephard, M. W., Clough, S. A., and Collins, W. D.: Radiative forcing by long-lived greenhouse gases: calculations with the AER radiative transfer models, *J. Geophys. Res.-Atmos.*, 113, D13103, doi:10.1029/2008JD009944, 2008.
- Knopf, D. A. and Koop, T.: Heterogeneous nucleation of ice on surrogates of mineral dust, *J. Geophys. Res.-Atmos.*, 111, D12201, doi:10.1029/2005JD006894, 2006.
- Koehler, K. A., Kreidenweis, S. M., DeMott, P. J., Petters, M. D., Prenni, A. J., and Möhler, O.: Laboratory investigations of the impact of mineral dust aerosol on cold cloud formation, *Atmos. Chem. Phys.*, 10, 11955–11968, doi:10.5194/acp-10-11955-2010, 2010.
- Kulkarni, G., Fan, J., Comstock, J. M., Liu, X., and Ovchinnikov, M.: Laboratory measurements and model sensitivity studies of dust deposition ice nucleation, *Atmos. Chem. Phys.*, 12, 7295–7308, doi:10.5194/acp-12-7295-2012, 2012.
- Langham, E. and Mason, B.: The heterogeneous and homogeneous nucleation of supercooled water, *P. Roy. Soc. Lond. A Mat.*, 247, 493–504, 1958.
- Linke, C., Möhler, O., Veres, A., Mohácsi, Á., Bozóki, Z., Szabó, G., and Schnaiter, M.: Optical properties and mineralogical composition of different Saharan mineral dust samples: a laboratory study, *Atmos. Chem. Phys.*, 6, 3315–3323, doi:10.5194/acp-6-3315-2006, 2006.
- Liu, X. and Penner, J. E.: Ice nucleation parameterization for global models, *Meteorol. Z.*, 14, 499–514, doi:10.1127/0941-2948/2005/0059, 2005.
- Liu, X., Penner, J. E., Ghan, S. J., and Wang, M.: Inclusion of ice microphysics in the NCAR Community Atmospheric Model Version 3 (CAM3), *J. Climate*, 20, 4526–4547, doi:10.1175/JCLI4264.1, 2007.
- Liu, X., Easter, R. C., Ghan, S. J., Zaveri, R., Rasch, P., Shi, X., Lamarque, J.-F., Gettelman, A., Morrison, H., Vitt, F., Conley, A., Park, S., Neale, R., Hannay, C., Ekman, A. M. L., Hess, P., Mahowald, N., Collins, W., Iacono, M. J., Bretherton, C. S., Flanner, M. G., and Mitchell, D.: Toward a minimal representation of aerosols in climate models: description and evaluation in the Community Atmosphere Model CAM5, *Geosci. Model Dev.*, 5, 709–739, doi:10.5194/gmd-5-709-2012, 2012a.
- Liu, X., Shi, X., Zhang, K., Jensen, E. J., Gettelman, A., Barahona, D., Nenes, A., and Lawson, P.: Sensitivity studies of dust ice nuclei effect on cirrus clouds with the Community Atmosphere Model CAM5, *Atmos. Chem. Phys.*, 12, 12061–12079, doi:10.5194/acp-12-12061-2012, 2012b.
- Lohmann, U. and Diehl, K.: Sensitivity studies of the importance of dust ice nuclei for the indirect aerosol effect on stratiform mixed-phase clouds, *J. Atmos. Sci.*, 63, 968–982, doi:10.1175/JAS3662.1, 2006.
- Lüönd, F., Stetzer, O., Welti, A., and Lohmann, U.: Experimental study on the ice nucleation ability of size-selected kaolinite particles in the immersion mode, *J. Geophys. Res.-Atmos.*, 115, D14201, doi:10.1029/2009JD012959, 2010.
- Määttänen, A., Vehkamäki, H., Lauri, A., Merikallio, S., Kauhanen, J., Savijärvi, H., and Kulmala, M.: Nucleation studies in the Martian atmosphere, *J. Geophys. Res.-Planet.*, 110, E02002, doi:10.1029/2004JE002308, 2005.
- Marcotelli, C., Gedamke, S., Peter, T., and Zobrist, B.: Efficiency of immersion mode ice nucleation on surrogates of mineral dust, *Atmos. Chem. Phys.*, 7, 5081–5091, doi:10.5194/acp-7-5081-2007, 2007.
- Meyers, M. P., DeMott, P. J., and Cotton, W. R.: New primary ice-nucleation parameterizations in an explicit cloud model, *J. Appl. Meteorol.*, 31, 708–721, doi:10.1175/1520-0450(1992)031<0708:NPINPI>2.0.CO;2, 1992.
- Möhler, O., Büttner, S., Linke, C., Schnaiter, M., Saathoff, H., Stetzer, O., Wagner, R., Krämer, M., Mangold, A., Ebert, V., and Schurath, U.: Effect of sulfuric acid coating on heterogeneous ice nucleation by soot aerosol particles, *J. Geophys. Res.-Atmos.*, 110, D11210, doi:10.1029/2004JD005169, 2005.
- Möhler, O., Field, P. R., Connolly, P., Benz, S., Saathoff, H., Schnaiter, M., Wagner, R., Cotton, R., Krämer, M., Mangold, A., and Heymsfield, A. J.: Efficiency of the deposition mode ice nucleation on mineral dust particles, *Atmos. Chem. Phys.*, 6, 3007–3021, doi:10.5194/acp-6-3007-2006, 2006.

- Möhler, O., Benz, S., Saathoff, H., Schnaiter, M., Wagner, R., Schneider, J., Walter, S., Ebert, V., and Wagner, S.: The effect of organic coating on the heterogeneous ice nucleation efficiency of mineral dust aerosols, *Environ. Res. Lett.*, 3, 025007, doi:10.1088/1748-9326/3/2/025007, 2008.
- Morrison, H. and Gettelman, A.: A new two-moment bulk stratiform cloud microphysics scheme in the Community Atmosphere Model, Version 3 (CAM3). Part I: Description and numerical tests, *J. Climate*, 21, 3642–3659, doi:10.1175/2008JCLI2105.1, 2008.
- Murray, B., O’Sullivan, D., Atkinson, J., and Webb, M.: Ice nucleation by particles immersed in supercooled cloud droplets, *Chem. Soc. Rev.*, 41, 6519–6554, 2012.
- Neale, R. B., Richter, J. H., and Jochum, M.: The impact of convection on ENSO: from a delayed oscillator to a series of events, *J. Climate*, 21, 5904–5924, 2008.
- Niedermeier, D., Hartmann, S., Shaw, R. A., Covert, D., Mentel, T. F., Schneider, J., Poulain, L., Reitz, P., Spindler, C., Clauss, T., Kiselev, A., Hallbauer, E., Wex, H., Mildenerger, K., and Stratmann, F.: Heterogeneous freezing of droplets with immersed mineral dust particles – measurements and parameterization, *Atmos. Chem. Phys.*, 10, 3601–3614, doi:10.5194/acp-10-3601-2010, 2010.
- Niedermeier, D., Shaw, R. A., Hartmann, S., Wex, H., Clauss, T., Voigtländer, J., and Stratmann, F.: Heterogeneous ice nucleation: exploring the transition from stochastic to singular freezing behavior, *Atmos. Chem. Phys.*, 11, 8767–8775, doi:10.5194/acp-11-8767-2011, 2011.
- Niedermeier, D., Ervens, B., Clauss, T., Voigtländer, J., Wex, H., Hartmann, S., and Stratmann, F.: A computationally efficient description of heterogeneous freezing: A simplified version of the Soccer ball model, *Geophys. Res. Lett.*, 41, 736–741., 2014.
- Niemand, M., Möhler, O., Vogel, B., Vogel, H., Hoose, C., Connolly, P., Klein, H., Bingemer, H., DeMott, P., Skrotzki, J., and Leisner, T.: A particle-surface-area-based parameterization of immersion freezing on desert dust particles, *J. Atmos. Sci.*, 69, 3077–3092, doi:10.1175/JAS-D-11-0249.1, 2012.
- Park, S. and Bretherton, C. S.: The University of Washington Shallow Convection and moist turbulence schemes and their impact on climate simulations with the Community Atmosphere Model, *J. Climate*, 22, 3449–3469, doi:10.1175/2008JCLI2557.1, 2009.
- Phillips, V. T. J., DeMott, P. J., and Andronache, C.: An empirical parameterization of heterogeneous ice nucleation for multiple chemical species of aerosol, *J. Atmos. Sci.*, 65, 2757–2783, doi:10.1175/2007JAS2546.1, 2008.
- Phillips, V. T. J., Demott, P. J., Andronache, C., Pratt, K. A., Prather, K. A., Subramanian, R., and Twohy, C.: Improvements to an Empirical Parameterization of Heterogeneous Ice Nucleation and Its Comparison with Observations, *J. Atmos. Sci.*, 70, 378–409, doi:10.1175/JAS-D-12-080.1, 2012.
- Pitter, R. L. and Pruppacher, H. R.: A wind tunnel investigation of freezing of small water drops falling at terminal velocity in air, *Q. J. Roy. Meteor. Soc.*, 99, 540–550, doi:10.1002/qj.49709942111, 1973.
- Prenni, A. J., DeMott, P. J., Kreidenweis, S. M., Harrington, J. Y., Avramov, A., Verlinde, J., Tjernström, M., Long, C. N., and Olsson, P. Q.: Can ice-nucleating aerosols affect arctic seasonal climate?, *B. Am. Meteorol. Soc.*, 88, 541–550, doi:10.1175/BAMS-88-4-541, 2007.
- Pruppacher, H. R., Klett, J. D., and Wang, P. K.: *Microphysics of Clouds and Precipitation*, Atmospheric and Oceanographic Sciences Library, Kluwer Academic Publishers, Dordrecht, the Netherlands, 1997.
- Richardson, M. S., DeMott, P. J., Kreidenweis, S. M., Cziczo, D. J., Dunlea, E. J., Jimenez, J. L., Thomson, D. S., Ashbaugh, L. L., Borys, R. D., Westphal, D. L., Casuccio, G. S., and Lersch, T. L.: Measurements of heterogeneous ice nuclei in the western United States in springtime and their relation to aerosol characteristics, *J. Geophys. Res.-Atmos.*, 112, D02209, doi:10.1029/2006JD007500, 2007.
- Rogers, D. C., DeMott, P. J., Kreidenweis, S. M., and Chen, Y.: A continuous-flow diffusion chamber for airborne measurements of ice nuclei, *J. Atmos. Ocean. Tech.*, 18, 725–741, doi:10.1175/1520-0426(2001)018<0725:ACFDCF>2.0.CO;2, 2001.
- Rosinski, J., Haagenson, P. L., Nagamoto, C. T., and Parungo, F.: Nature of ice-forming nuclei in marine air masses, *J. Aerosol Sci.*, 18, 291–309, doi:10.1016/0021-8502(87)90024-3, 1987.
- Rosinski, J., Nagamoto, C. T., and Zhou, M. Y.: Ice-forming nuclei over the East China Sea, *Atmos. Res.*, 36, 95–105, doi:10.1016/0169-8095(94)00029-D, 1995.
- Seland, Ø., Iversen, T., Kirkevåg, A., and Storelvmo, T.: Aerosol-climate interactions in the CAM-Oslo atmospheric GCM and investigation of associated basic shortcomings, *Tellus A*, 60, 459–491, doi:10.1111/j.1600-0870.2008.00318.x, 2008.
- Sullivan, R. C., Petters, M. D., DeMott, P. J., Kreidenweis, S. M., Wex, H., Niedermeier, D., Hartmann, S., Clauss, T., Stratmann, F., Reitz, P., Schneider, J., and Sierau, B.: Irreversible loss of ice nucleation active sites in mineral dust particles caused by sulphuric acid condensation, *Atmos. Chem. Phys.*, 10, 11471–11487, doi:10.5194/acp-10-11471-2010, 2010.
- Vali, G.: Nucleation terminology, *J. Aerosol Sci.*, 16, 575–576, 1985.
- Wang, M., Ghan, S., Ovchinnikov, M., Liu, X., Easter, R., Kasianov, E., Qian, Y., and Morrison, H.: Aerosol indirect effects in a multi-scale aerosol-climate model PNNL-MMF, *Atmos. Chem. Phys.*, 11, 5431–5455, doi:10.5194/acp-11-5431-2011, 2011.
- Welti, A., Lüönd, F., Kanji, Z. A., Stetzer, O., and Lohmann, U.: Time dependence of immersion freezing: an experimental study on size selected kaolinite particles, *Atmos. Chem. Phys.*, 12, 9893–9907, doi:10.5194/acp-12-9893-2012, 2012.
- Wheeler, M. J. and Bertram, A. K.: Deposition nucleation on mineral dust particles: a case against classical nucleation theory with the assumption of a single contact angle, *Atmos. Chem. Phys.*, 12, 1189–1201, doi:10.5194/acp-12-1189-2012, 2012.
- Wiacek, A. and Peter, T.: On the availability of uncoated mineral dust ice nuclei in cold cloud regions, *Geophys. Res. Lett.*, 36, L17801, doi:10.1029/2009GL039429, 2009.
- Xie, S., Boyle, J., Klein, S. A., Liu, X., and Ghan, S.: Simulations of Arctic mixed-phase clouds in forecasts with CAM3 and AM2 for M-PACE, *J. Geophys. Res.-Atmos.*, 113, D04211, doi:10.1029/2007JD009225, 2008.
- Xie, S., Liu, X., Zhao, C., and Zhang, Y.: Sensitivity of CAM5-simulated Arctic clouds and radiation to ice nucleation parameterization, *J. Climate*, 26, 5981–5999, doi:10.1175/JCLI-D-12-00517.1, 2013.

- Young, K. C.: The role of contact nucleation in ice phase initiation in clouds, *J. Atmos. Sci.*, 31, 768–776, doi:10.1175/1520-0469(1974)031<0768:TROCNI>2.0.CO;2, 1974.
- Zender, C. S., Bian, H., and Newman, D.: Mineral Dust Entrainment and Deposition (DEAD) model: description and 1990s dust climatology, *J. Geophys. Res.-Atmos.*, 108, 4416, doi:10.1029/2002JD002775, 2003.
- Zhang, G. J. and McFarlane, N. A.: Sensitivity of climate simulations to the parameterization of cumulus convection in the Canadian Climate Centre general circulation model, *Atmos. Ocean*, 33, 407–446, 1995.
- Zimmermann, F., Weinbruch, S., Schütz, L., Hofmann, H., Ebert, M., Kandler, K., and Wörringen, A.: Ice nucleation properties of the most abundant mineral dust phases, *J. Geophys. Res.-Atmos.*, 113, 8576, doi:10.1029/2008JD010655, 2008.
- Zobrist, B., Koop, T., Luo, B. P., Marcolli, C., and Peter, T.: Heterogeneous ice nucleation rate coefficient of water droplets coated by a nonadecanol monolayer, *J. Phys. Chem. C*, 111, 2149–2155, doi:10.1021/jp066080w, 2007.